nature genetics

ARTICLES

https://doi.org/10.1038/s41588-020-0652-z

Check for updates

Genomic analyses implicate noncoding de novo variants in congenital heart disease

Felix Richter[1,31], Sarah U. Morton[2,3,31], Seong Won Kim[4,31], Alexander Kitaygorodsky[5,31], Lauren K. Wasson[4,31], Kathleen M. Chen[6,31], Jian Zhou[6,7,8], Hongjian Qi[5], Nihir Patel[9], Steven R. DePalma[4], Michael Parfenov[4], Jason Homsy[4,10], Joshua M. Gorham[4], Kathryn B. Manheimer[1,11], Matthew Velinder[12], Andrew Farrell[12], Gabor Marth[12], Eric E. Schadt[9,11,13], Jonathan R. Kaltman[14], Jane W. Newburger[15], Alessandro Giardini[16], Elizabeth Goldmuntz[17,18], Martina Brueckner[19], Richard Kim[20], George A. Porter Jr.[21], Daniel Bernstein[22], Wendy K. Chung[23], Deepak Srivastava[24,32], Martin Tristani-Firouzi[25,32], Olga G. Troyanskaya[6,7,26,32], Diane E. Dickel[27,32], Yufeng Shen[5,32], Jonathan G. Seidman[4,32], Christine E. Seidman[4,28,32] and Bruce D. Gelb[9,29,30,32] ✉

A genetic etiology is identified for one-third of patients with congenital heart disease (CHD), with 8% of cases attributable to coding de novo variants (DNVs). To assess the contribution of noncoding DNVs to CHD, we compared genome sequences from 749 CHD probands and their parents with those from 1,611 unaffected trios. Neural network prediction of noncoding DNV transcriptional impact identified a burden of DNVs in individuals with CHD ($n = 2,238$ DNVs) compared to controls ($n = 4,177$; $P = 8.7 \times 10^{-4}$). Independent analyses of enhancers showed an excess of DNVs in associated genes (27 genes versus 3.7 expected, $P = 1 \times 10^{-5}$). We observed significant overlap between these transcription-based approaches (odds ratio (OR) = 2.5, 95% confidence interval (CI) 1.1–5.0, $P = 5.4 \times 10^{-3}$). CHD DNVs altered transcription levels in 5 of 31 enhancers assayed. Finally, we observed a DNV burden in RNA-binding-protein regulatory sites (OR = 1.13, 95% CI 1.1–1.2, $P = 8.8 \times 10^{-5}$). Our findings demonstrate an enrichment of potentially disruptive regulatory noncoding DNVs in a fraction of CHD at least as high as that observed for damaging coding DNVs.

CHD, which occurs in 1% of live births, has seen marked improvements in survival with modern surgical and medical management[1]. The decrease in infant mortality has increased CHD prevalence in older individuals and has exposed comorbidities that impair quality of life and life expectancy. Elucidation of CHD etiologies may improve outcomes, so the National Heart, Lung, and Blood Institute (NHLBI)-funded Pediatric Cardiac Genomics Consortium (PCGC) recruited >13,000 patients and utilized whole-exome sequencing (WES) and chromosome microarrays to study CHD genetic architecture. Our analyses identified damaging rare transmitted variants and DNVs in 8% of patients with sporadic CHD (including 28% of syndromic and 3% of isolated CHD)[2–5].

[1]Graduate School of Biomedical Sciences, Icahn School of Medicine at Mount Sinai, New York, NY, USA. [2]Department of Pediatrics, Harvard Medical School, Boston, MA, USA. [3]Division of Newborn Medicine, Boston Children's Hospital, Boston, MA, USA. [4]Department of Genetics, Harvard Medical School, Boston, MA, USA. [5]Departments of Systems Biology and Biomedical Informatics, Columbia University, New York, NY, USA. [6]Flatiron Institute, Simons Foundation, New York, NY, USA. [7]Lewis-Sigler Institute for Integrative Genomics, Princeton University, Princeton, NJ, USA. [8]Lyda Hill Department of Bioinformatics, University of Texas Southwestern Medical Center, Dallas, TX, USA. [9]Department of Genetics and Genomic Sciences, Icahn School of Medicine at Mount Sinai, New York, NY, USA. [10]Center for External Innovation, Takeda Pharmaceuticals USA, Cambridge, MA, USA. [11]Sema4, Stamford, CT, USA. [12]Department of Human Genetics, Utah Center for Genetic Discovery, University of Utah School of Medicine, Salt Lake City, UT, USA. [13]Icahn Institute for Genomics and Multiscale Biology, Icahn School of Medicine at Mount Sinai, New York, NY, USA. [14]Heart Development and Structural Diseases Branch, Division of Cardiovascular Sciences, NHLBI/NIH, Bethesda, MD, USA. [15]Boston Children's Hospital, Boston, MA, USA. [16]Cardiorespiratory Unit, Great Ormond Street Hospital, London, UK. [17]Division of Cardiology, Children's Hospital of Philadelphia, Philadelphia, PA, USA. [18]Department of Pediatrics, The Perelman School of Medicine, University of Pennsylvania, Philadelphia, PA, USA. [19]Departments of Pediatrics and Genetics, Yale University School of Medicine, New Haven, CT, USA. [20]Children's Hospital Los Angeles, Los Angeles, CA, USA. [21]Department of Pediatrics, University of Rochester, Rochester, NY, USA. [22]Department of Pediatrics, Stanford University, Palo Alto, CA, USA. [23]Departments of Pediatrics and Medicine, Columbia University Medical Center, New York, NY, USA. [24]Gladstone Institute of Cardiovascular Disease and University of California San Francisco, San Francisco, CA, USA. [25]Division of Pediatric Cardiology, University of Utah School of Medicine, Salt Lake City, UT, USA. [26]Department of Computer Science, Princeton University, Princeton, NJ, USA. [27]Environmental Genomics and Systems Biology Division, Lawrence Berkeley National Lab, Berkeley, CA, USA. [28]Department of Cardiology, Brigham and Women's Hospital, Boston, MA, USA. [29]Mindich Child Health and Development Institute, Icahn School of Medicine at Mount Sinai, New York, NY, USA. [30]Department of Pediatrics, Icahn School of Medicine at Mount Sinai, New York, NY, USA. [31]These authors contributed equally: Felix Richter, Sarah U. Morton, Seong Won Kim, Alexander Kitaygorodsky, Lauren K. Wasson, Kathleen M. Chen. [32]These authors jointly supervised this work: Deepak Srivastava, Martin Tristani-Firouzi, Olga G. Troyanskaya, Diane E. Dickel, Yufeng Shen, Jonathan G. Seidman, Christine E. Seidman, Bruce D. Gelb. ✉e-mail: bruce.gelb@mssm.edu

Many DNVs identified in patients with CHD alter proteins that function in chromatin modification, regulation of transcription and RNA processing[4].

On the basis of these findings, we reasoned that additional causes of CHD may reside in noncoding elements that are functional during cardiac development. To explore this, we performed whole-genome sequencing (WGS) to identify single nucleotide variants (SNVs) and small insertions or deletions (indels) in 763 CHD trios comprised of affected probands and unaffected parents and in 1,611 child–parent trios without CHD. First, 14 CHD probands with previously undetected probable causal genetic variants were identified; then, we compared noncoding DNVs in the remaining cohort using three approaches. Two strategies focused on cardiac gene regulatory elements; one that used a neural network model that predicts variant-level resolution functional impact and the other that involved analysis of multiple DNVs in genes with human fetal heart enhancers that overlap cardiomyocyte differentiation open chromatin. We identified significant overlap between results from these complementary approaches and confirmed differences in transcription activity for 5 of 31 variants tested. Our third strategy, which interrogated RNA processing, found significant enrichment of noncoding DNVs in individuals with CHD (cases). Finally, we observed potentially contributory noncoding DNVs in isolated CHD probands as well as those with neurodevelopmental delays or extracardiac anomalies, suggesting varying degrees of cardiac specificity. Taken together, these results demonstrate a noncoding DNV contribution to CHD that is mediated through transcriptional and post-transcriptional regulatory effects on cardiac development.

Results

Trio cohort characteristics and sequencing. We performed WGS (30× coverage) on 763 CHD probands (311 with extracardiac anomalies and 452 with isolated heart malformations) and unaffected parents enrolled by the PCGC (Supplementary Table 1a and phenotype summary in Supplementary Table 1b)[2]. Samples were subjected to WGS if prior WES studies[5] failed to identify rare damaging missense or loss-of-function coding variants in CHD genes (Supplementary Table 5). We also studied DNVs in 1,611 individuals without CHD or autism, who had siblings with autism, and their parents, from the Simons Simplex Collection[6]. To ensure accurate variant detection, DNVs were identified using the Genome Analysis Toolkit (GATK) and were further evaluated with FreeBayes[7] local realignment, followed by classification by a neural network trained on Integrated Genomics Viewer (IGV) plots[8] and manual curation of ambiguous variants (Methods; Supplementary Tables 2 and 3). PCR-based Sanger sequencing validated 98% of 266 de novo SNVs and 94% of 83 de novo indels in cases. In controls, 94% of de novo SNVs were present in at least one published analysis (Extended Data Fig. 1)[9,10]. We identified a mean of 71 de novo SNVs and 5 de novo indels per CHD proband (58,090 DNVs) and 68 de novo SNVs and 5 de novo indels per control individual (117,344 DNVs), which is consistent with WGS data obtained on similar platforms and with similar coverage[11].

As expected, the number of DNVs per individual correlated with paternal ($\beta_{CHD}=1.4$, $P_{CHD}=5\times10^{-54}$; $\beta_{control}=1.4$, $P_{control}=6\times10^{-86}$) and maternal ($\beta_{CHD}=0.5$, $P_{CHD}=2\times10^{-5}$; $\beta_{control}=0.4$, $P_{control}=3\times10^{-8}$) ages (multiple variable linear regression; Extended Data Fig. 2)[11,12]. SNVs drove this association, but there was also a de novo indel association with paternal ($\beta_{CHD}=0.07$, $P_{CHD}=2\times10^{-4}$; $\beta_{control}=0.05$, $P_{control}=3\times10^{-4}$) but not maternal ($\beta_{CHD}=0.01$, $P_{CHD}=0.6$; $\beta_{control}=0.03$, $P_{control}=0.1$) age[13]. Without parental age adjustment, cases had more DNVs per individual than did controls ($P=2\times10^{-9}$, two-sided Student's *t*-test), but this was not the case after adjustment ($P=0.1$). To account for this difference, comparisons were made with respect to the total number of DNVs in CHD probands and controls.

Coding de novo variants identified by whole-exome sequencing and whole-genome sequencing. WES data were available for 612 of 763 CHD probands[4,5]. Among 628 coding DNVs, including 582 within WES capture regions (lifted over[14] to hg38), both WES and WGS identified 509 (81%), whereas 38 of 69 DNVs called only by WES were confirmed by WGS IGV visualization (Supplementary Note). Fifty coding DNVs identified solely by WGS (8%; 0.08/proband) included 4 within and 46 outside WES capture regions. One DNV that was initially called by WES was removed for low read depth; three were not called by WES but were confirmed by WES IGV visualization.

These analyses defined damaging DNVs in established CHD genes (*PTPN11*, *NOTCH1* ($n=2$), *FBN1*, *FLT4*, *NR2F2* and *GATA4*), and identified six individuals with 22q11 copy number variants and one with trisomy 21. The proband with a previously reported pathogenic *FBN1* DNV in exon 42 (1-00761) had mitral stenosis, brachycephaly, short stature and other features consistent with geleophysic dysplasia (MIM 614185), 50% of cases of which are caused by damaging DNVs in *FBN1* exon 41 or 42. Damaging DNVs in known CHD genes were confirmed with reference-free DNV calling (Methods) and IGV visualization. Six potentially damaging DNVs were identified in candidate CHD genes, including one insertion that was detected only with reference-free calling (Supplementary Table 4), but these individuals were retained for noncoding analyses. Following the exclusion of probands with probable causal genetics, 749 CHD probands were analyzed for noncoding DNVs.

Quantitative burden with categorical de novo variant classifications. We observed no noncoding DNV enrichment in 749 CHD trios for DNVs that are associated with human ($n=210$) or mouse ($n=614$) CHD genes or genes that are highly expressed in heart development ($n=4,420$) (Supplementary Tables 5 and 6). Similarly, we observed no enrichment in noncoding cardiac regulatory features comprising transcription factor binding sites ($n_{human}=8$, $n_{mouse}=45$), histone marks ($n_{human}=45$, $n_{mouse}=60$) and DNase hypersensitivity sites ($n_{human}=23$, $n_{mouse}=3$) assayed on cardiac cells ($n_{human}=15$), prenatal or fetal heart tissue ($n_{human}=26$, $n_{mouse}=34$) and postnatal heart tissue ($n_{human}=35$, $n_{mouse}=74$) (Methods; Extended Data Fig. 3 and Supplementary Table 7)[15–32].

Qualitative burden with HeartENN. As we found no genome-wide significant DNV burden in global regions of cardiac transcriptional regulation among CHD probands, we predicted impact with variant-level resolution. We developed HeartENN (Heart Effect Neural Network; Fig. 1), an extension of DeepSEA[33], which predicts molecular effect differences between any two alleles for every regulatory feature by using convolutional neural networks. Another DeepSEA extension successfully identified noncoding DNV enrichment in autism[9]. HeartENN was trained on a 1,000-bp genomic sequence context with the same 184 cardiac noncoding regulatory features that were used for previous region-based burden tests, but not those that were used for subsequent multiple-hit analysis (Methods; Supplementary Table 7). Aside from using cardiac epigenomic training data and extending these to mouse features, HeartENN is similar to DeepSEA. The HeartENN mean receiver operator characteristic area under the curves (ROC AUCs) for mouse and human features were 0.9 and 0.85, respectively, similar to the ROC AUCs of DeepSEA; the area under the precision-recall curves were also comparable (Extended Data Fig. 4). We restricted our analysis to heart-related features and defined no other hypotheses of relevance to CHD. The maximum functional difference score observed in any feature was assigned to each DNV (Supplementary Table 8).

We defined a range of scores relevant to congenital defects by contrasting maximum functional difference scores between

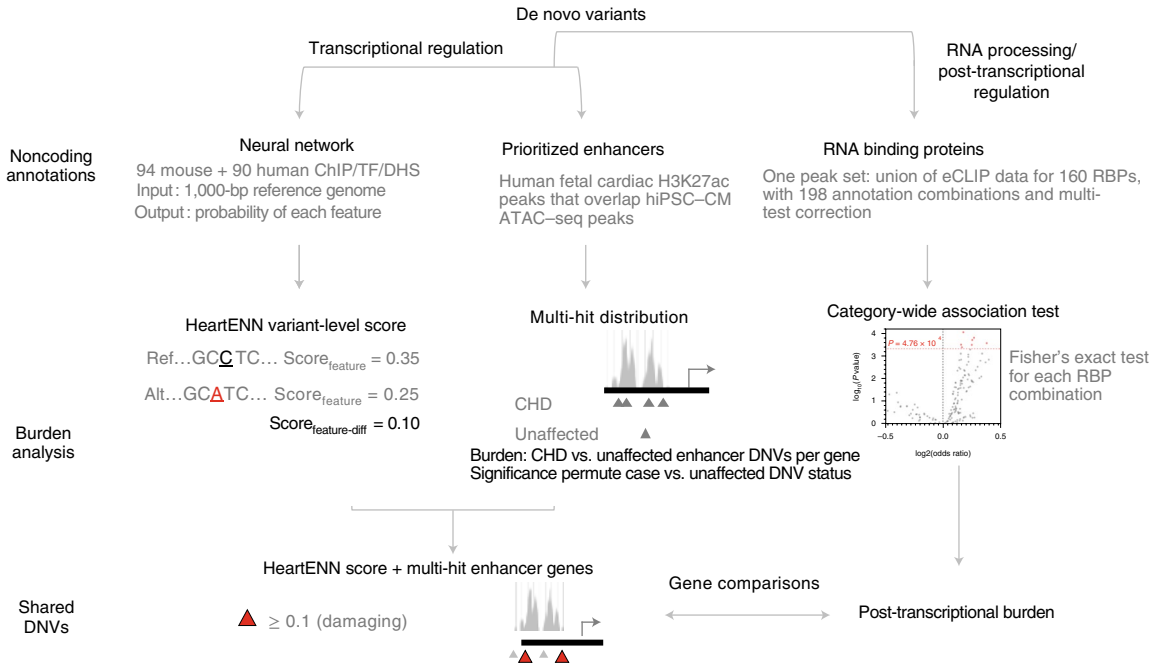

Fig. 1 | Analysis schematic. Overview of the approach to identifying a noncoding de novo variant burden in CHD. TF, transcription factor; DHS, DNase hypersensitivity sites; NS, not significant.

Human Gene Mutation Database (HGMD) regulatory mutations ($n=1{,}564$), inclusive of congenital defect pathogenic variants, and regulatory polymorphisms ($n=642$). Because these variants occur in individuals with diverse malformations, we evaluated signals using DeepSEA[9,33], which is generalizable to multiple organ systems. Pathogenic variants, but not polymorphisms, had an excess of DeepSEA scores ≥0.1 (Extended Data Fig. 5a). As we lacked an equivalent dataset of CHD noncoding variants with which to evaluate HeartENN, we compared the DeepSEA and HeartENN null distributions. After randomly down-sampling DeepSEA to match the number of HeartENN annotations and applying HGMD polymorphism scores, we observed similar null distributions for HeartENN and DeepSEA (Extended Data Fig. 5b). We therefore set HeartENN scores of ≥0.1 as potentially biologically meaningful for CHD.

The majority (>96%) of DNVs had HeartENN scores <0.1, which suggests that there is little functional impact from most variants. CHD cases were enriched for HeartENN scores ≥0.1 ($n=2{,}238$ DNVs in CHD, $n=4{,}177$ DNVs in controls, Fisher's exact test $P=8.7\times10^{-4}$, OR = 1.09, 95% confidence interval (CI) 1.04–1.15, attributable risk (AR) = 183/2,283 DNVs). We tested enrichment across multiple cut-off points, and observed (1) no marginal ($P<0.05$) significance in controls at any cut-off, (2) higher ORs with stricter thresholds (Fig. 2a and Supplementary Table 9), and (3) significance when all thresholds were accounted for (Fig. 2b; permutation $P=1.7\times10^{-3}$, 10,000 permutations). Above 0.25, we observed consistent positive effect sizes despite decreased sample sizes, which suggests a lack of power with more stringent thresholds. To test whether the signal was consistent across functionally significant HeartENN scores, we placed every DNV into 0.02-HeartENN-score bins. We calculated the difference in fraction of DNVs in every 0.02 bin (Fig. 2c) and observed a strong propensity toward cases across bins.

We tested whether other noncoding variant prioritization methods ranked HeartENN-damaging (score ≥ 0.1) variants as pathogenic. There was statistically significant support from all algorithms tested (LINSIGHT[34], CADD[35,36], DeepSEA[9,33], GERP++ (ref. [37]) and GWAVA TSS[38]) (Extended Data Fig. 6). We observed a case–control burden with CADD ≥ 15 ($P_{\text{Bonferroni}}=0.019$), albeit without a dose-response relationship or cardiac-relevant interpretation.

Gene set enrichment of DNVs with HeartENN ≥ 0.1 upstream or downstream (<1 kb) or within 5′-UTR, intronic or 3′-UTR sequences showed enrichment of known human CHD genes in cases (Fig. 2d and Supplementary Table 10; $n=18/959$ genes in cases and $n=10/1{,}704$ genes in controls, OR = 3.2, 95% CI 1.4–7.9, hypergeometric one-sided $P=5.7\times10^{-4}$). Notably, one proband with isolated CHD had a DNV (maximum HeartENN score 0.15, ID 1-07589) within a previously validated *GATA4* enhancer with heart-constrained activity (Vista ID hs2205, heart-specific in 6 of 7 embryonic day (E)11.5 embryos)[27].

Burden of genes with multiple de novo variants in human fetal cardiac enhancers. A second approach involved the interrogation of noncoding DNVs and focused on regions that were experimentally implicated in human cardiac developmental gene expression regulation. This strategy harnessed 31,555 human fetal heart enhancers identified by H3K27ac chromatin immunoprecipitation (ChIP) of human fetal cardiac tissues (8–17 weeks post-conception; Methods). None was included in the HeartENN analysis. We intersected these fetal cardiac enhancers with open chromatin sequences obtained by assay for transposase-accessible chromatin using sequencing (ATAC–seq) during the differentiation of human induced pluripotent stem cells into cardiomyocytes (hiPSC–CMs). On the basis of prototypic gene expression, ATAC–seq was performed at two differentiation states: cardiac mesoderm (day 8; 155,989 ATAC peaks) and primordial cardiomyocytes (day 17; 62,326 ATAC peaks). The subset of ATAC peaks that overlapped cardiac enhancers defined 21,618 prioritized human fetal heart enhancers (Supplementary Table 11). We assessed these sequences for DNVs.

Among the prioritized human fetal heart enhancers, we identified 2,427 DNVs in CHD cases and 5,160 DNVs in controls (Fisher's exact $P=1$; Supplementary Table 12). Assignment of nearest genes defined 1,793 genes in CHD cases and 3,195 genes in controls. Among CHD cases, 27 genes were marginally enriched for DNVs. No gene was enriched for DNVs in controls (Fig. 3a and

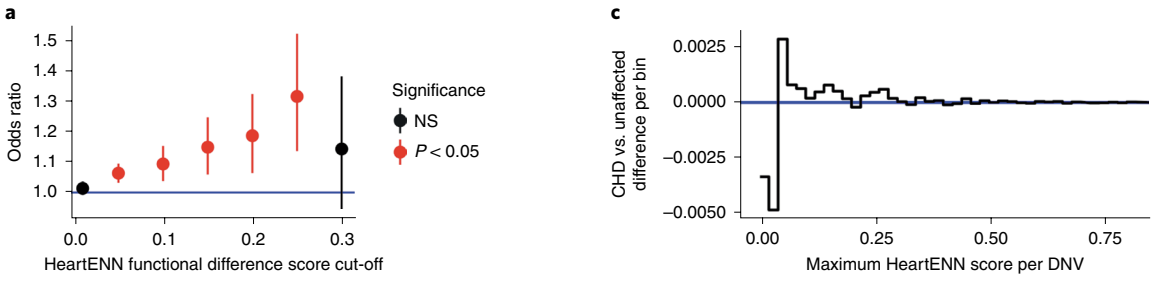

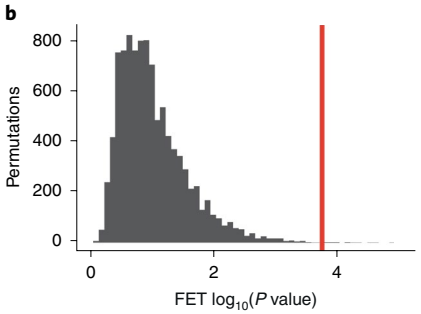

d

Human CHD gene	Variants (hg38)	Maximum HeartENN score	Maximum HeartENN feature
BCOR	ChrX:40146952:TTCCGCC>T	0.241	CTCF Human cardiomyocyte lineage
STAMBP	Chr2:73839781:A>G	0.264	CTCF Human cardiomyocyte lineage
SEMA3E	Chr7:83553143:C>T	0.450	CTCF Mouse heart tissue
UBR1	Chr15:43073086:G>A	0.291	CTCF Mouse heart tissue
OFD1	ChrX:13734718:A>G	0.261	H3K27ac Human right ventricle

Fig. 2 | Enrichment of noncoding de novo variants with functionally relevant HeartENN scores. a, The number of noncoding DNVs above various HeartENN thresholds (*x* axis) was counted in individuals with CHD ($n=749$) and in unaffected individuals ($n=1,611$) and these were compared to the total number of scored DNVs in individuals with CHD ($n=56,164$) and in unaffected individuals ($n=114,065$), plotted as ORs with 95% CI (counts, ORs and Fisher's exact test two-sided unadjusted *P* values are listed in Supplementary Table 9). **b**, Permutations of case–control status ($n=10,000$, gray) found a significant *P* value when all cut-offs were accounted for ($P=1.7\times10^{-3}$, one-sided) by comparing the most significant observed *P* value (red) to the most significant *P* value per permutation (gray). **c**, The fraction of DNVs in 0.02-HeartENN-score bins demonstrated consistent propensity toward cases for functionally relevant HeartENN bins. **d**, Known human CHD genes with HeartENN-damaging (score ≥ 0.1) DNVs were enriched in CHD ($n_{CHD}=18$, $n_{unaffected}=10$, OR = 3.2, hypergeometric one-sided $P=6\times10^{-4}$), with the top 5 (shown here) predicted to disrupt CTCF and H3K27ac features. FET, Fisher's exact test.

Supplementary Table 13). In 10^5 permutations of randomly assigned case or control status, fewer genes exhibited DNV enrichment than was observed ($P<1\times10^{-5}$; Fig. 3b).

These 27 genes were associated with 99 case DNVs and 13 control DNVs (Supplementary Table 14). Nine case DNVs (but none in controls) had HeartENN scores ≥0.1 (Supplementary Table 14), which is significantly more than the <4% expected by chance (one-sided hypergeometric $P=5.4\times10^{-3}$; Fig. 3c). Significance was assessed using the null hypothesis of proportional overlap, which was appropriate, as the HeartENN analysis used different cardiac epigenomic data from the prioritized human fetal heart enhancers. Ten of the 27 genes that were enriched for DNVs in prioritized human fetal heart enhancers were highly expressed in E14.5 mouse hearts ($P=0.06$): *COL1A2*, *MAPRE2*, *SEPTIN11*, *PSMA7*, *SORBS1*, *RPL25P1*, *FILIP1*, *MITF*, *SUN1* and *ATE1* (Supplementary Table 13). Twelve genes (*FNIP1*, *COL1A2*, *MITF*, *MAPRE2*, *PSMA7*, *LRRTM2*, *NAB1*, *SUN1*, *SEPTIN11*, *MARCHF3*, *RPL29* and *ATE1*) had a modest probability of loss-of-function variant intolerance (pLI) of >0.5 ($P=0.03$), on the basis of variant prevalence in the Exome Aggregation Consortium (ExAC)[39]. One gene (*COL1A2*) was observed at the intersection of these findings: it includes a HeartENN ≥ 0.1 DNV, has a high pLI and is highly expressed during mouse heart development. *COL1A2* encodes a collagen that is highly expressed in developing cardiac valves[36]. Among the seven individuals with *COL1A2*-associated human fetal heart enhancer DNVs, all had pulmonary and/or aortic valve abnormalities, which indicates an enrichment trend compared to the 742 participants without such DNVs (486/742, $P=0.05$).

Functional effects of de novo variation on transcriptional activity. We assessed the potential transcriptional effects of 31 DNVs (Fig. 4a) that were identified by HeartENN, and/or the prioritized human fetal heart enhancers, using massively parallel reporter assays (MPRAs)[40]. Paired sequences (300–1,600 bp) containing reference or DNV sequences were synthesized and introduced into a pMPRA1 plasmid. At least three independent plasmid libraries were produced and transfected into multiple wells of iPSC–CMs at differentiation day 17 or day 37. Transcriptional activity was assessed by comparing RNA and DNA test sequence reads per well. We observed no significant differences in transcriptional activity by construct length (Extended Data Fig. 7). Five of 31 construct pairs showed significant mean differences between the reference and DNV sequences for at least three replicates (Fig. 4; two-sided Student's *t*-test, Benjamini–Hochberg-adjusted $P<0.05$), including two DNVs that increased transcriptional activity. Two additional pairs showed transcriptional differences between DNV and reference sequences for two replicates, but no overall statistical significance (Extended Data Fig. 8). These seven MPRA-positive variants were among 18 that were identified by both HeartENN (score ≥ 0.1) and prioritized human fetal heart enhancers or by HeartENN (score ≥ 0.1) and ATAC–seq peaks. Among 13 variants that were selected with a single bioinformatic approach, none reproducibly showed significant MPRA differences.

Post-transcriptional regulatory enrichment. In addition to transcriptional regulatory disruption, we tested the effect of noncoding DNV enrichment on post-transcriptional regulation. RNA-binding proteins (RBPs) mediate post-transcriptional regulation through pre-mRNA splicing, transport, localization, degradation and translational control. We obtained 160 RBP enhanced cross-linking immunoprecipitation (eCLIP) datasets from two ENCODE cell lines[15]. Because there are no cardiac eCLIP data, we inferred transcriptionally active cardiac binding sites by overlapping the human fetal heart H3K36me3 active transcription mark

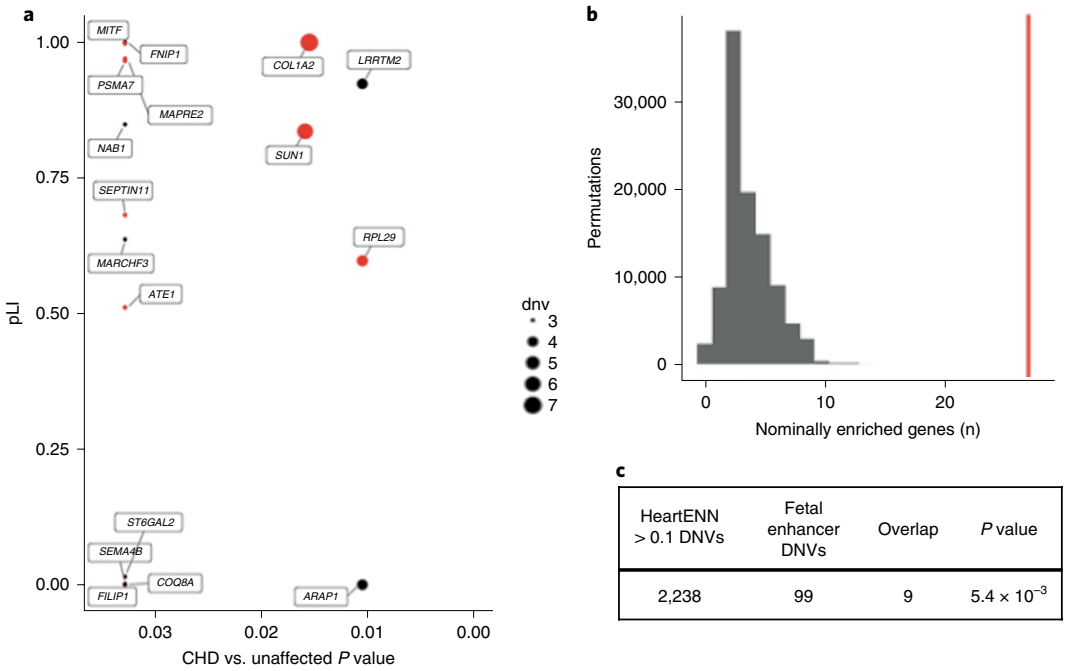

c

HeartENN > 0.1 DNVs	Fetal enhancer DNVs	Overlap	*P* value
2,238	99	9	5.4×10^{-3}

d

Gene	Variants with HeartENN ≥ 0.1 (hg38)	Top HeartENN feature
COQ8A	Chr1:226963471:C>T	CTCF (mouse heart tissue)
ARAP1	Chr11:72752280:A>G	DNase HS (human cardiomyocyte lineage)
COL1A2	Chr7:94366906:G>GGA	GATA4 TFBS (mouse heart tissue)
SEMA4B	Chr15:90193048:G>C	DNase HS (human atrial fibroblast lineage)
	Chr15:90191832:G>A	DNase HS (mouse heart tissue)
ATXN1	Chr6:16761717:G>A	CTCF (human cardiomyocyte lineage)
	Chr6:16521783:C>T	H3K27me3 (mouse heart tissue)
MIR4656	Chr7:4796340:C>T	CTCF (mouse heart tissue)
MIR4774	Chr2:168633306:A>T	DNase HS (human atrial fibroblast lineage)

Fig. 3 | Genes with multiple de novo variants in prioritized human fetal heart enhancers. a, Genes with a burden of DNVs in associated fetal cardiac enhancers with $P < 0.05$ for individuals with CHD ($n = 749$) compared to those in unaffected indviduals ($n = 1,611$). For each gene, the DNV burden *P* value (*x* axis) was determined with a two-sided Fisher's exact test that compared DNVs in individuals with CHD ($n = 56,164$) with those in unaffected individuals ($n = 114,065$) and is plotted against the pLI (*y* axis). Dot size reflects the number of DNVs in the CHD cohort and red denotes genes in the upper quartile of gene expression during heart development. Five genes without pLI values are not shown. **b**, Distribution of the number of nominally enriched genes by 100,000 random permutations of DNVs within prioritized human fetal heart enhancers demonstrates significant enrichment of genes with a burden of CHD DNVs. As there were never 21 genes observed (red) in the permutation test, the most extreme *P* value would be 10^{-5} (one-sided). **c**, Overlap between DNVs with HeartENN score ≥ 0.1 ($n = 2,238$) and those within prioritized human fetal heart enhancers ($n = 99$) is significantly enriched in CHD (one-sided hypergeometric distribution and no overlapping DNVs in controls). **d**, Top features representing a diverse spectrum of transcriptional regulation.

(used in HeartENN) and human embryonic stem cells (not used in HeartENN or prioritized human fetal heart enhancers). We used this narrower RBP binding site definition to test the noncoding burden for all 162 annotation combinations (Fig. 5a). These included the following: H3K36me3 histone mark, SNV and/or indel, constrained or haploinsufficient gene proximity, and transcription start site (TSS) or 3′-UTR anchor. The number of independent tests, determined with eigenvalue decomposition, was used to determine the Bonferroni *P* value multiple testing adjustment[41]. This provided 105 independent tests with significance threshold $P = 4.76 \times 10^{-4}$.

We observed a significant enrichment of RBP DNVs overlapping H3K36me3 marks (Fig. 5b,c). The most significant result was that of RBP variants overlapping H3K36me3 in ES-UCSF4 stem cells (OR = 1.13, 95% CI 1.1–1.2, two-sided Fisher's exact test $P = 8.77 \times 10^{-5}$, 1,672 case DNVs; Supplementary Table 15). The signal was statistically significant for multiple embryonic stem cell types and when limited to constrained genes or TSS proximity. When these biologically relevant features were intersected, the largest statistically significant effect size was obtained (OR = 1.3, 95% CI 1.1–1.5, $P = 2.68 \times 10^{-4}$, 327 case DNVs).

We tested variant-level intersections between these post-transcriptional and transcriptional regulatory results. For the most significant RBP-implicated DNVs, there was a statistically significant overlap with DNVs in prioritized human fetal heart enhancers in cases ($n = 10$, OR = 3.6, 95% CI 1.9–∞, hypergeometric one-sided $P = 2.1 \times 10^{-4}$) but not in controls ($n = 0$). There was no significant overlap between RBP-implicated and HeartENN-damaging (score ≥ 0.1) DNVs in cases ($n = 78$, OR = 1.21, 95% CI 1.0–∞, $P = 0.05$) or controls ($n = 122$, OR = 1.12, 95% CI 0.9–∞, $P = 0.10$). By contrast, for RBP-implicated DNVs in constrained regions, we

a

Bioinformatic selection	No. of pairs tested	$P_{adjusted} < 0.05$
Fetal heart prioritized (FHP)	5	0
HeartENN ≥ 0.5	8	0
HeartENN ≥ 0.1 + ATAC	11	3
HeartENN ≥ 0.1 + FHP	7	2
Total	31	5

b

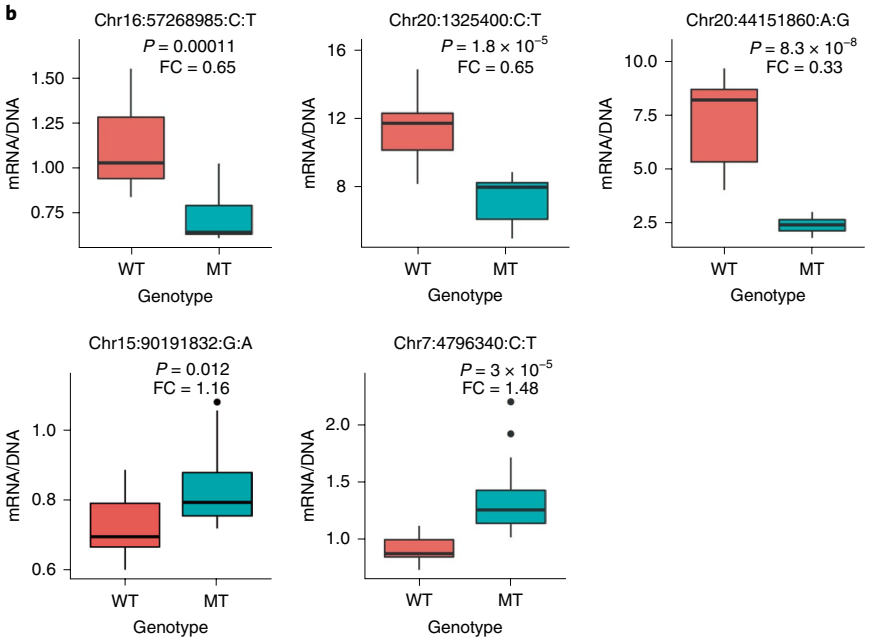

c

Variants (hg38)	Prioritized by	HeartENN	Gene
1–00046:chr7:4796340C>T	HeartENN + FHP	0.139	*AP5Z1*
1–13185:chr20:44151860A>G	HeartENN + ATAC	0.277	*JPH2*
1–07009:chr20:1325400C>T	HeartENN + ATAC	0.182	*SDCBP2*
1–06412:chr16:57268985C>T	HeartENN + ATAC	0.149	*PLLP*
1–08416:chr15:90191832G>A	HeartENN + FHP	0.103	*SEMA4B*

Fig. 4 | Massively parallel reporter assays for selected de novo variants. a, Pairs of reference and DNV sequences were selected on the basis of bioinformatic analyses for the following classes: prioritized human fetal heart enhancer only, high HeartENN score (≥0.5) only, HeartENN score ≥ 0.1 at an ATAC-seq peak, and HeartENN score ≥ 0.1 in a prioritized human fetal heart enhancer. The numbers of pairs tested and the numbers for which the DNV sequence resulted in significantly different levels of transcription are indicated. **b**, Box plots for the five pairs for which the transcription level from the DNV (MT) was significantly different from the reference (WT) sequence. Box plots show the median fold change (FC), first and third quartiles (lower and upper hinges) and range of values (whiskers and outlying points). Both **a** and **b** show two-sided Student's *t*-test Benjamini–Hochberg *P* values; each boxplot has at least 3 independent experiments with 4 technical replicates each, and the HeartENN ≥ 0.1 + FHP group was repeated 4 times. **c**, The genomic positions of the five DNVs for which transcription was significantly altered are indicated along with their bioinformatic classes, HeartENN functional difference scores and associated genes.

observed only one case DNV that intersected with prioritized fetal human heart enhancers and we observed a statistically significant overlap with HeartENN-DNVs in cases ($n = 19$, OR = 1.52, 95% CI 1.0–∞, $P = 0.033$) but not in controls ($n = 16$, OR = 0.86, 95% CI 0.5–∞, $P = 0.7$). Thus, in addition to transcriptional regulatory disruption, we found evidence that disturbed post-transcriptional regulation machinery may contribute to CHD.

Distribution of noncoding de novo variants in canonical variant classes. We characterized DNVs in canonical variant classes (intronic, promoter, UTR and so on) for HeartENN-damaging (score ≥ 0.1) DNVs, prioritized human fetal heart enhancer multiple-hit DNVs and post-transcriptional regulatory-disrupting DNVs (Extended Data Fig. 9). The majority of DNVs that were not identified by any bioinformatic method were intergenic (52% in

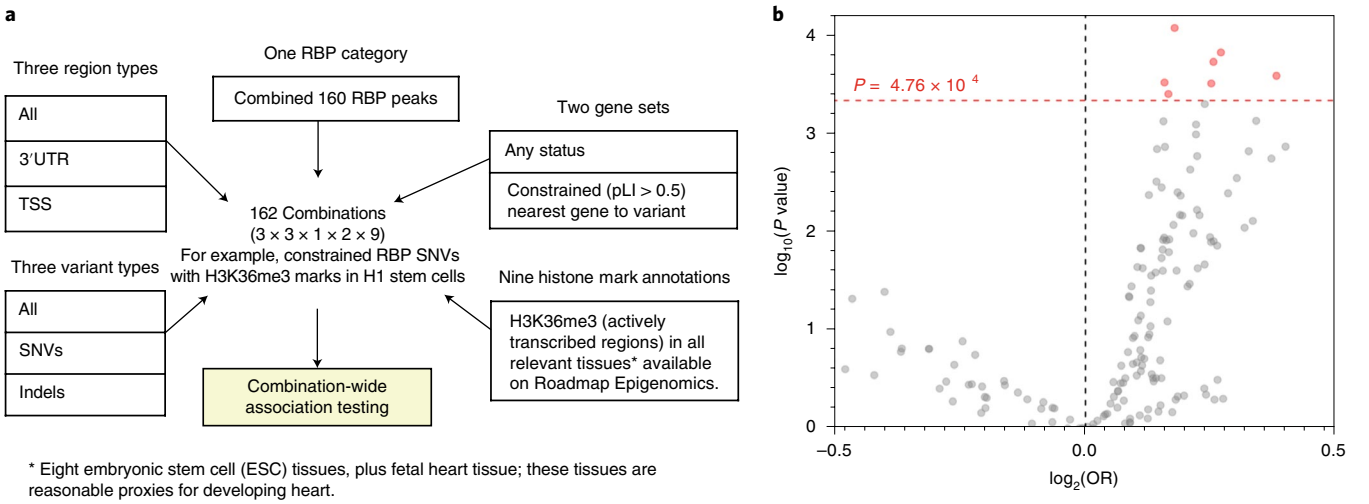

c

Highlighted tests

Feature combination	Variants	Hits, cases	Hits, controls	n_1 (cases)	n_0 (controls)	OR	95% CI	*P* value
RBP H3K36me3 in ES-UCSF4 cells	SNVs	1,672	3,040	52,004	106,438	1.13	(1.06, 1.20)	8.77×10^{-5}
TSS RBP H3K36me3 in H1 cells	SNVs	686	1,169	52,004	106,438	1.20	(1.09, 1.32)	1.55×10^{-4}
TSS RBP H3K36me3 in ES-UCSF4 cells	SNVs	740	1,274	52,004	106,438	1.19	(1.09, 1.31)	1.94×10^{-4}
Constrained TSS RBP H3K36me3 in H1 cells	SNVs	327	516	52,004	106,438	1.30	(1.13, 1.50)	2.68×10^{-4}
RBP H3K36me3 in ES-UCSF4 cells	SNV + indel	1,797	3,291	55,827	113,467	1.11	(1.05, 1.18)	3.13×10^{-4}
TSS RBP H3K36me3 in HUES64 cells	SNVs	713	1,231	52,004	106,438	1.19	(1.08, 1.30)	3.20×10^{-4}
RBP H3K36me3 in H1 cells	SNVs	1,568	2,874	52,004	106,438	1.12	(1.05, 1.19)	4.10×10^{-4}

Fig. 5 | Enrichment of variants in RNA-binding-protein category annotations. a, Five groups of annotations were defined to investigate post-transcriptional regulation through disruption of RBP binding, which resulted in $n = 162$ combinations of (1) variant type; (2) region type; (3) RBP category; (4) gene sets, specifically pLI constraint on nearest gene; and (5) histone mark annotations for actively transcribed regions in relevant proxy tissues. These annotation categories were considered in the category-wide association test and provided 105 independent tests, giving 4.76×10^{-4} as the strict Bonferroni threshold. **b**, Variant enrichment and significance for each test category, determined with a two-sided Fisher's exact test: SNV-only tests used a total of $n_1 = 52{,}004$ case SNVs and $n_0 = 106{,}438$ control SNVs; SNV + indel tests used a total $n_1 = 55{,}827$ case variants and $n_0 = 113{,}467$ control variants. The association tests that passed Bonferroni significance have been highlighted in red. **c**, Detailed tabulation of the seven Bonferroni-significant Fisher's exact tests (two-sided).

cases and 52% in controls). By contrast, variants that were prioritized by the three methods were more likely to be intronic, with over-representation among other canonical categories depending on the method. This provides additional evidence that CHD-associated noncoding DNVs may have functional effects.

Recurrently implicated genes with noncoding de novo variants. Among the union of implicated noncoding DNVs (HeartENN-damaging DNVs (2,238 cases and 4,177 controls), prioritized human fetal heart enhancer multiple-hit DNVs (99 cases and 13 controls) and post-transcriptional regulatory-disrupting DNVs from all seven Bonferroni-significant enrichments (2,149 cases and 3,963 controls)), 25 genes were recurrently implicated (unadjusted two-sided binomial $P < 0.05$) (Supplementary Table 16). High-interest genes were identified with haploinsufficiency constraint (pLI > 0.5 or missense *Z*-score > 3), high mouse E14.5 heart expression rank, human or mouse CHD gene membership and CHD-associated KEGG pathway membership. Results included two human CHD genes, but corresponding probands did not have the characteristic CHD phenotype of pulmonic stenosis. Candidate genes included *SHOC2* (human CHD gene and constrained), *ZNRF3, CPSF3* (CHD-associated KEGG pathway and constrained) and *MAP4K4* (96th percentile embryonic heart expression and constrained).

Association between candidate noncoding de novo variants and neurodevelopmental disorders or extracardiac anomalies. We tested whether implicated noncoding DNVs were associated with the following phenotypic subgroups: isolated CHD ($n = 298$), CHD with neurodevelopmental disorders (NDD) ($n = 267$) or CHD with extracardiac anomalies (ECA) ($n = 305$). Compared to probands with WES-identified damaging DNVs in highly expressed cardiac genes, CHD probands with DNVs in the 27 genes associated with prioritized human fetal heart enhancers had a lower frequency of NDD (odds 20/53 versus 113/119; OR = 0.40, 95% CI 0.2–0.7, $P = 0.002$) but a similar prevalence of ECA (34/39 versus 173/184; OR = 0.92, 95% CI 0.5–1.6, $P = 0.87$).

In contrast to probands with prioritized human fetal heart enhancer DNVs, most probands had at least one HeartENN-damaging (score ≥ 0.1) DNV, and presumably only a minority would be associated with CHD. Therefore, we tested phenotype associations by comparing HeartENN-damaging DNV enrichment within subgroups to that in controls (Extended Data Fig. 10a). A consistent enrichment was observed across all subgroups. We then tested the hypothesis that the parent algorithm, DeepSEA, which previously implicated noncoding DNVs in autism[9], would also identify a burden in CHD cases with NDDs. No significant association was observed, but the highest effect size was observed for CHD with NDDs (OR = 1.05, 95% C.I. 1.0–1.1, two-sided Fisher's exact test $P = 0.18$). A similarly consistent enrichment within subgroups was observed for RBP-implicated DNVs (Extended Data Fig. 10b).

Contribution to congenital heart disease. We estimated the mean AR to CHD in the WES-negative cohort across all three methods (Methods), assuming at most one causal, functional DNV per proband. HeartENN-damaging (score ≥ 0.1) DNVs contributed to a

maximum of 24% of cases of CHD in this cohort, and enrichment decreased with increasing HeartENN cut-offs (11% attributed to HeartENN ≥ 0.2 and 2.9% attributed to HeartENN ≥ 0.3). This resulted in a final HeartENN contribution range of 3–24%. DNVs in prioritized human fetal heart enhancers contributed to 12.1% of cases of CHD, including 1.1% that was attributable to shared HeartENN ≥ 0.1 DNVs. Lower percentages for DNVs associated with genes with pLI > 0.5 (5.4%) or high embryonic mouse heart expression (3.8%) resulted in a contribution range of 4–12%. Finally, DNVs that were implicated in post-transcriptional disruption contributed to 10% of CHD in this cohort. Although the cumulative percentage mean attributed risk (17–45%) suggests that a substantial contribution is made by DNVs in WES-negative CHD, these estimates must be refined in future studies. In summary, the fraction of CHD cases with contributory noncoding predicted functional DNVs in this WES-negative cohort is at least as high as the fraction of CHD cases with damaging coding DNVs identified with WES.

Discussion

Noncoding variants remain potential contributors to disorders with unexplained genetics. Using WGS, we tested this hypothesis through systematic examination of noncoding regulatory elements in a mutation-negative CHD cohort. We, like others[41–44], observed a lack of significant findings across broad noncoding annotation categories. By contrast, our alternative interrogation of noncoding variants implicated noncoding DNVs in CHD pathogenesis.

HeartENN, which provides variant-level scores, as does the multifaceted DeepSEA algorithm that uncovered noncoding DNVs in autism[9], defined significantly more DNVs in CHD probands. Separate analyses of prioritized human fetal heart enhancers identified distinct and some overlapping DNVs in CHD cases. Notably, functional assays were positive when these two strategies were combined. Although there was no transcriptional regulatory category-wide burden, we observed a Bonferroni-significant category-wide burden among heart-transcribed RBP binding sites. These data implicate noncoding DNVs in CHD at both the transcriptional and post-transcriptional regulatory levels. Our ability to detect signals was strongly influenced by the availability of cardiovascular development noncoding genomic data, which permitted us a narrow search space for DNV interrogation.

Through the two cardiac regulatory element strategies and their significant overlapping results, we identified known and potential human CHD genes. HeartENN-damaging variants were enriched for known human CHD genes (for example, *GATA4* and *OFD1*), but there was little concordance between observed and reported cardiac/extracardiac phenotype constellations. Only one of seven genes identified with both approaches is implicated in heart development: *COL1A2* encodes a collagen that is highly expressed in developing cardiac valves[45], and all seven probands with noncoding *COL1A2* DNVs had pulmonary and/or aortic valve abnormalities. Whether the other overlapping genes represent novel CHD genes or poor understanding of the genic regulation of noncoding DNVs remains uncertain. Among 20 nonoverlapping genes with multi-DNV enrichment in prioritized human fetal heart enhancers, 4 are implicated in heart development: *ATE1* depletion causes CHD in mice[46]; *LRRTM2* resides within a CHD-associated region[47]; *MITF* regulates *GATA4* expression[48,49]; and *RPL29* encodes a target of LSD, a demethylase whose depletion causes CHD in mice[50,51]. Other gene associations include cardiomyopathy (*FNIP1*)[52], striated muscle disorders (*SUN1*)[53,54] and mouse embryonic lethality (*SEPTIN11*)[55]. When considering the union of transcriptional and post-transcriptional variants, *SHOC2*, *CPSF3*, *ZNRF3* and *MAP4K4* regulatory regions were consistently identified.

Among 31 DNV-containing sequences that were functionally tested in iPSC–CMs, 5 (16%) significantly altered transcription. Whereas that rate is consistent with bioinformatic enrichment analyses, there are reasons to consider this a lower bound. The sequences were only tested in fetal cardiomyocytes at two time points using minimal promoters not in their native genomic context. Oligogenetic effects were not modeled in this functional assay. Genes associated with the five positive DNVs provide clues regarding CHD causality. *JPH2* encodes junctophlilin-2, a membrane protein necessary for T-tubule formation, for which an N-terminal cleavage fragment modulates MEF2-mediated gene transcription, altering ERK and TGF-β signaling[56]. *SEMA4B* is in the top quartile for gene expression in the developing heart and encodes a semaphorin that signals through plexin receptors. Perturbations in semaphorin–plexin signaling can lead to CHD[57,58]. Future studies of additional DNVs incorporating more complex models will be needed to elaborate CHD pathogenesis precisely.

Our cohort was selected for WES-negative trios and higher paternal age to increase statistical power to identify a noncoding and de novo signal, respectively. Among this CHD cohort, we estimated that the fraction of individuals harboring noncoding predicted functional DNVs that contribute to CHD is at least as high as the fraction of CHD cases with contributory coding DNVs. We observed consistent results in isolated CHD cases and in those with NDDs or ECAs, which is distinctly different from the NDD and ECA enrichment among CHD probands with damaging coding DNVs. For the prioritized human fetal heart enhancer DNVs, this manifested as depletion in the number of patients with CHD and NDD compared to those with WES-implicated coding DNVs. These results could be explained by cardiac-specific effects in at least a subset of DNVs, which suggests that future work could build on the cardiac relevance described here with a focus on cardiac specificity. The implicated *GATA4* enhancer in a proband with isolated CHD illustrates the potential to uncouple frequently associated phenotypes through cardiac-selective regulatory effects.

Although our findings established that noncoding DNVs contribute to CHD pathogenesis, the relevant genetic mechanisms remain to be explored. Previous studies of rare coding variants suggested that some are sufficient to engender CHD (that is, by a Mendelian genetic model), whereas many others are associated with incomplete penetrance, which suggests greater genetic complexity (for example, an oligogenic model) and/or environment effects[59]. Whereas noncoding DNVs that contribute to CHD could act in a simple Mendelian manner (for instance, substantially reducing allelic expression), more modest gene expression effects would be congruous with an oligogenic mechanism. Future studies of noncoding variants observed in CHD are needed to establish transcriptional effect sizes and their ability to perturb heart development individually and in concert with other relevant factors.

These data systematically associate human CHD with cardiac regulatory DNVs. Our findings highlight the potential of WGS to more fully elucidate the genetic architecture of CHD. Extension of the statistical framework used is likely to define additional noncoding variants in CHD. When this strategy is applied to larger cohorts, we expect to refine the magnitude of noncoding effects and to investigate complex CHD genetics, such as epistatic and pleiotropic effects of noncoding and coding variants.

Online content

Any methods, additional references, Nature Research reporting summaries, source data, extended data, supplementary information, acknowledgements, peer review information; details of author contributions and competing interests; and statements of data and code availability are available at https://doi.org/10.1038/s41588-020-0652-z.

Received: 9 March 2019; Accepted: 22 May 2020;
Published online: 29 June 2020

References

1. van der Linde, D. et al. Birth prevalence of congenital heart disease worldwide. *J. Am. Coll. Cardiol.* **58**, 2241–2247 (2011).
2. Pediatric Cardiac Genomics Consortium et al.The Congenital Heart Disease Genetic Network Study: rationale, design, and early results. *Circ. Res.* **112**, 698–706 (2013).
3. Zaidi, S. et al. De novo mutations in histone-modifying genes in congenital heart disease. *Nature* **498**, 220–223 (2013).
4. Homsy, J. et al. De novo mutations in congenital heart disease with neuro-developmental and other congenital anomalies. *Science* **350**, 1262–1266 (2015).
5. Jin, S. C. et al. Contribution of rare inherited and de novo variants in 2,871 congenital heart disease probands. *Nat. Genet.* **49**, 1593–1601 (2017).
6. Fischbach, G. D. & Lord, C. The Simons Simplex Collection: a resource for identification of autism genetic risk factors. *Neuron* **68**, 192–195 (2010).
7. Garrison, E. & Marth, G. Haplotype-based variant detection from short-read sequencing. Preprint at https://arxiv.org/abs/1207.3907v2 (2012).
8. Richter, F. et al. Whole genome de novo variant identification with FreeBayes and neural network approaches. Preprint at *bioRxiv* https://doi.org/10.1101/2020.03.24.994160 (2020).
9. Zhou, J. et al. Whole-genome deep-learning analysis identifies contribution of noncoding mutations to autism risk. *Nat. Genet.* **51**, 973–980 (2019).
10. An, J.-Y. et al. Genome-wide de novo risk score implicates promoter variation in autism spectrum disorder. *Science* **362**, eaat6576 (2018).
11. Jónsson, H. et al. Parental influence on human germline de novo mutations in 1,548 trios from Iceland. *Nature* **549**, 519–522 (2017).
12. Goldmann, J. M. et al. Parent-of-origin-specific signatures of de novo mutations. *Nat. Genet.* **48**, 935–939 (2016).
13. Seiden, A. H. et al. Elucidation of de novo small insertion/deletion biology with parent-of-origin phasing. *Hum. Mutat.* **41**, 800–806 (2020).
14. Kent, W. J. et al. The human genome browser at UCSC. *Genome Res.* **12**, 996–1006 (2002).
15. Bernstein, B. E. et al. An integrated encyclopedia of DNA elements in the human genome. *Nature* **489**, 57–74 (2012).
16. Mei, S. et al. Cistrome Data Browser: a data portal for ChIP–Seq and chromatin accessibility data in human and mouse. *Nucleic Acids Res.* **45**, D658–D662 (2017).
17. He, A. et al. Dynamic GATA4 enhancers shape the chromatin landscape central to heart development and disease. *Nat. Commun.* **5**, 4907 (2014).
18. Sayed, D., Yang, Z., He, M., Pfleger, J. M. & Abdellatif, M. Acute targeting of general transcription factor IIB restricts cardiac hypertrophy via selective inhibition of gene transcription. *Circ. Heart Fail.* **8**, 138–148 (2015).
19. Stefanovic, S. et al. GATA-dependent regulatory switches establish atrioventricular canal specificity during heart development. *Nat. Commun.* **5**, 3680 (2014).
20. Sayed, D., He, M., Yang, Z., Lin, L. & Abdellatif, M. Transcriptional regulation patterns revealed by high resolution chromatin immunoprecipitation during cardiac hypertrophy. *J. Biol. Chem.* **288**, 2546–2558 (2013).
21. Zhang, L. et al. KLF15 establishes the landscape of diurnal expression in the heart. *Cell Rep.* **13**, 2368–2375 (2015).
22. Anand, P. et al. BET bromodomains mediate transcriptional pause release in heart failure. *Cell* **154**, 569–582 (2013).
23. Attanasio, C. et al. Tissue-specific SMARCA4 binding at active and repressed regulatory elements during embryogenesis. *Genome Res.* **24**, 920–929 (2014).
24. Sakabe, N. J. et al. Dual transcriptional activator and repressor roles of TBX20 regulate adult cardiac structure and function. *Hum. Mol. Genet.* **21**, 2194–2204 (2012).
25. Consortium, R. E. et al. Integrative analysis of 111 reference human epigenomes. *Nature* **518**, 317–330 (2015).
26. May, D. et al. Large-scale discovery of enhancers from human heart tissue. *Nat. Genet.* **44**, 89–93 (2012).
27. Dickel, D. E. et al. Genome-wide compendium and functional assessment of in vivo heart enhancers. *Nat. Commun.* **7**, 12923 (2016).
28. Nord, A. S. et al. Rapid and pervasive changes in genome-wide enhancer usage during mammalian development. *Cell* **155**, 1521–1531 (2013).
29. Blow, M. J. et al. ChIP–Seq identification of weakly conserved heart enhancers. *Nat. Genet.* **42**, 806–810 (2010).
30. Yue, F. et al. A comparative encyclopedia of DNA elements in the mouse genome. *Nature* **515**, 355–364 (2014).
31. Shen, Y. et al. A map of the *cis*-regulatory sequences in the mouse genome. *Nature* **488**, 116–120 (2012).
32. van den Boogaard, M. et al. Genetic variation in T-box binding element functionally affects *SCN5A*/*SCN10A* enhancer. *J. Clin. Invest.* **122**, 2519–2530 (2012).
33. Zhou, J. & Troyanskaya, O. G. Predicting effects of noncoding variants with deep learning–based sequence model. *Nat. Methods* **12**, 931–934 (2015).
34. Huang, Y.-F., Gulko, B. & Siepel, A. Fast, scalable prediction of deleterious noncoding variants from functional and population genomic data. *Nat. Genet.* **49**, 618–624 (2017).
35. Kircher, M. et al. A general framework for estimating the relative pathogenicity of human genetic variants. *Nat. Genet.* **46**, 310–315 (2014).
36. Rentzsch, P., Witten, D., Cooper, G. M., Shendure, J. & Kircher, M. CADD: predicting the deleteriousness of variants throughout the human genome. *Nucleic Acids Res.* **47**, D886–D894 (2019).
37. Davydov, E. V. et al. Identifying a high fraction of the human genome to be under selective constraint using GERP++. *PLoS Comput. Biol.* **6**, e1001025 (2010).
38. Ritchie, G. R. S., Dunham, I., Zeggini, E. & Flicek, P. Functional annotation of noncoding sequence variants. *Nat. Methods* **11**, 294–296 (2014).
39. Lek, M. et al. Analysis of protein-coding genetic variation in 60,706 humans. *Nature* **536**, 285–291 (2016).
40. Melnikov, A., Zhang, X., Rogov, P., Wang, L. & Mikkelsen, T. S. Massively parallel reporter assays in cultured mammalian cells. *J. Vis. Exp.* https://doi.org/10.3791/51719 (2014).
41. Werling, D. M. et al. An analytical framework for whole-genome sequence association studies and its implications for autism spectrum disorder. *Nat. Genet.* **50**, 727–736 (2018).
42. Turner, T. N. et al. Genomic patterns of de novo mutation in simplex autism. *Cell* **171**, 710–722.e12 (2017).
43. C Yuen, R. K. et al. Whole genome sequencing resource identifies 18 new candidate genes for autism spectrum disorder. *Nat. Neurosci.* **20**, 602–611 (2017).
44. Hamdan, F. F. et al. High rate of recurrent de novo mutations in developmental and epileptic encephalopathies. *Am. J. Hum. Genet.* **101**, 664–685 (2017).
45. Peacock, J. D., Lu, Y., Koch, M., Kadler, K. E. & Lincoln, J. Temporal and spatial expression of collagens during murine atrioventricular heart valve development and maintenance. *Dev. Dyn.* **237**, 3051–3058 (2008).
46. Kurosaka, S. et al. Arginylation regulates myofibrils to maintain heart function and prevent dilated cardiomyopathy. *J. Mol. Cell. Cardiol.* **53**, 333–341 (2012).
47. Kleffmann, W. et al. 5q31 microdeletions: definition of a critical region and analysis of *LRRTM2*, a candidate gene for intellectual disability. *Mol. Syndromol.* **3**, 68–75 (2012).
48. Mehta, G. et al. MITF interacts with the SWI/SNF subunit, BRG1, to promote GATA4 expression in cardiac hypertrophy. *J. Mol. Cell. Cardiol.* **88**, 101–110 (2015).
49. Tshori, S. et al. Transcription factor MITF regulates cardiac growth and hypertrophy. *J. Clin. Invest.* **116**, 2673–2681 (2006).
50. Nicholson, T. B. et al. A hypomorphic lsd1 allele results in heart development defects in mice. *PLoS One* **8**, e60913 (2013).
51. Hamidi, T. et al. Identification of Rpl29 as a major substrate of the lysine methyltransferase Set7/9. *J. Biol. Chem.* **293**, 12770–12780 (2018).
52. Siggs, O. M. et al. Mutation of *Fnip1* is associated with B-cell deficiency, cardiomyopathy, and elevated AMPK activity. *Proc. Natl Acad. Sci. USA* **113**, E3706–E3715 (2016).
53. Chen, C.-Y. et al. Accumulation of the inner nuclear envelope protein Sun1 is pathogenic in progeric and dystrophic laminopathies. *Cell* **149**, 565–577 (2012).
54. Meinke, P. et al. Muscular dystrophy-associated *SUN1* and *SUN2* variants disrupt nuclear-cytoskeletal connections and myonuclear organization. *PLoS Genet.* **10**, e1004605 (2014).
55. Röseler, S. et al. Lethal phenotype of mice carrying a *Sept11* null mutation. *Biol. Chem.* **392**, 779–781 (2011).
56. Guo, A. et al. E–C coupling structural protein junctophilin-2 encodes a stress-adaptive transcription regulator. *Science* **362**, eaan3303 (2018).
57. Yamagishi, H. et al. A history and interaction of outflow progenitor cells implicated in "Takao Syndrome." In *Etiology and Morphogenesis of Congenital Heart Disease: From Gene Function and Cellular Interaction to Morphology* (eds. Nakanishi, T. et al.) 201–209 (Springer, 2016).
58. Masuda, T. & Taniguchi, M. Congenital diseases and semaphorin signaling: overview to date of the evidence linking them. *Congenit. Anom. (Kyoto).* **55**, 26–30 (2015).
59. Pierpont, M. E. et al. Genetic basis for congenital heart disease: revisited: a scientific statement from the American Heart Association. *Circulation* **138**, e653–e711 (2018).

Publisher's note Springer Nature remains neutral with regard to jurisdictional claims in published maps and institutional affiliations.

© The Author(s), under exclusive licence to Springer Nature America, Inc. 2020

Methods

Participants. *Pediatric Cardiac Genomics Consortium.* Patients with structural CHD and their parents ($n=763$ trios) were enrolled in the PCGC Congenital Heart Disease Network Study (CHD GENES: ClinicalTrials.gov identifier NCT01196182)[2]. The protocols were approved by the Institutional Review Boards of Boston's Children's Hospital, Brigham and Women's Hospital, Children's Hospital of Los Angeles, Children's Hospital of Philadelphia, Columbia University Medical Center, Great Ormond Street Hospital, Icahn School of Medicine at Mount Sinai, Rochester School of Medicine and Dentistry, Steven and Alexandra Cohen Children's Medical Center of New York and Yale School of Medicine. All participants or their parents provided informed consent. Individuals with a chromosomal aneuploidy, copy number variation associated with CHD or probable causal variant identified with WES were excluded. The echocardiogram, catheterization and operative reports were reviewed to determine cardiac phenotypes. Extracardiac structural anomalies were obtained from the medical records. Patients were classified as having neurodevelopmental disorders (NDDs) if parents reported the presence of developmental delay, learning disability, mental retardation or autism for individuals at least 12 months old.

Controls. Controls comprised 1,611 sibling–parent trios, unaffected by CHD or autism, derived from sporadic autism quartets that consisted of one offspring with autism, one unaffected sibling and their unaffected parents[6]. Controls were ascertained from 1,627 siblings after excluding 16 with a past medical history that included CHD. The Simons Foundation kindly provided the phenotypic and genomic data for these unaffected trios.

Whole-genome sequencing and variant identification. DNA from the PCGC samples was sequenced at the Baylor College of Medicine Genomic and RNA Profiling Core ($n=900$), the New York Genome Center (NYGC) Genomic Research Services ($n=75$), and the Broad Institute for Genomic Services ($n=1,314$) following the same protocol. Genomic DNA from venous blood or saliva was prepared for sequencing using a PCR-free library preparation ($n=2,289$) or SK2-IES library preparation ($n=75$, Broad Institute). All samples were sequenced on an Illumina Hi-Seq X Ten system with 150-bp paired reads to a median depth of >30× per individual. The controls were prepared in a manner similarl to that of cases. Specifically, the controls were sequenced at NYGC ($n=4,833$) with 150-bp paired reads and a median depth of >30× per individual, using either a PCR-based library preparation on an Illumina Hi-Seq 2000 ($n=114$) or a PCR-free library preparation on an Illumina Hi-Seq X Ten ($n=4,719$). Previous Simons Simplex Collection sequencing of controls was performed at NYGC on the Illumina Hi-Seq 2500 ($n=120$) or the Illumina Hi-Seq X Ten ($n=4,761$) to >30× coverage with 150-bp paired reads.

For both cases and controls, reads were aligned to GRCh37 or GRCh38 with the Burrows-Wheeler Aligner (BWA-MEM)[60]. GATK best practices recommendations were implemented for base quality score recalibration, indel realignment, and duplicate removal[61]. Standard hard filtering parameters were used for SNV and indel discovery across all 763 PCGC and 1,611 control trios, followed by $N+1$ joint genotyping and variant quality score recalibration[62,63].

Identification and confirmation of de novo variants. DNV identification was performed for both cases and controls by pooling three pipelines from PCGC members at Mount Sinai, Columbia and Harvard. Mount Sinai used two tiers; a high stringency tier and a low stringency tier. High stringency tier parameters were as follows: GATK PASS (that is, variants were classified as true with an adaptive error model based on known true sites and artifacts); heterozygous ratio (AB) set to 0.3–0.7 in the proband; homozygous ratio (AB) less than 0.01 in both parents; depth (DP) ≥ 10; joint genotyping allele count (AC) = 1 across all trios; genotype quality (GQ) > 60 (proband and parents); alternate allele depth (AAD) > 7 in the proband and AAD < 3 in each parent. The lower tier consisted of de novo calls that fell outside the higher tier and that did not fail the following filters: GATK PASS; heterozygous AB set to 0.2–0.8; DP = 7–120; AC = 1 in all trios; GQ > 60 (proband); GQ > 30 (parents) and AAD > 7. At Columbia, parameters for DNV identification were as follows: heterozygous or homozygous for the alternate allele in the proband; homozygous for the reference allele in the parents; not in a multiallelic site (3 or more); AC ≤ 2 in the cohort; Fisher's exact test strand bias (FS) < 25; variant quality by depth (QD) > 2 for SNVs and QD > 1 for indels; ReadPosRankSum > −3 for indels; proband genotype Phred-scaled likelihood (PL) ≥ 70; proband AAD ≥ 6; proband heterozygous AB ≥ 0.28 if AAD ≥ 10 or heterozygous AB ≥ 0.20 if AAD < 10; parental GQ ≥ 30; parental DP ≥ 10; parental AB < 0.035 and a population frequency of <0.1% (in the 1000 Genomes, Exome Sequencing Project and ExAC populations). For the third pipeline, at Harvard, the parameters were as follows: AC = 1; DP = 7–64 inclusive; ADD ≥ 5; heterozygous AB = 0.2–0.8 inclusive and homozygous AB ≤ 0.1. Putative de novo calls near indels, in a homopolymer indel or in a dinucleotide repeat were subsequently visually filtered with IGV. After consolidation of de novo calls, all variants were force-called with FreeBayes[7]. GATK and FreeBayes both perform local realignment. GATK uses a combination of known common variants, indels and entropy calculations to generate log of the odds ratio (LOD) scores for alternative consensus sequences, replacing original alignments if LOD scores are higher. FreeBayes generalizes this Bayesian caller approach to allow for multiallelic loci and non-uniform copy number across samples, and the combination of GATK and FreeBayes variant calling was previously reported to improve the positive predictive value of indel identification to >97% (ref. [64]). Therefore, FreeBayes variant calling was performed on GATK-identified DNVs to reduce false-positive variants. DNVs that occurred in the high evidence tier at Mount Sinai, but which were false with FreeBayes, were manually reviewed. Finally, IGV plots of all the putative DNVs were passed through an eight-layer convolutional neural network trained on curated IGV plots, and were classified into six categories (de novo SNVs, de novo insertions, de novo deletions, complex, uncertain and false positives)[8]. Predicted false positives were excluded. Predicted de novo insertion, deletion, complex and uncertain events were subject to further manual inspection to remove additional false positives. DNVs with ExAC allele frequency > 0.1% as well as DNVs in nonstandard chromosomes, segmental duplications (score ≥ 0.99), low complexity regions, low mappability (300 bp, score < 1) regions, mucin or human leukocyte antigen genes, and ENCODE-blacklisted sites were removed[15,65–67]. Finally, all DNVs within 50 bp in the same proband were considered to be a single event (that is, a mutation cluster) for region-based and multiple-hit enrichment tests. DNVs identified using the GRCh37 genome assembly were lifted over to GRCh38 (ref. [14]). Sanger sequencing validation was performed for 266 de novo SNVs and 83 de novo indels.

Reference-free calling to identify candidate coding de novo variants. An alternative, reference-free DNV calling algorithm, RUFUS (https://github.com/jandrewrfarrell/RUFUS)[68], was also used to call de novo variants in PCGC probands. In brief, RUFUS compares the *k*-mer sequences directly from the raw Illumina reads of the proband–parent trio to identify unique DNA sequences present in the child that represent de novo genetic variation. Sequencing reads that contain these unique *k*-mer sequences are assembled using an inbuilt sequence assembler. Assembled contigs, which contain the de novo allele, are mapped back to the human reference sequence for localization, using the BWA algorithm. RUFUS then interprets the aligned contigs to produce a VCF-formatted variant report. All types of de novo variation (SNVs, short indels and structural variants of all types) are identified in a single run of the program.

Gene sets. The three gene sets used in this study were genes in which coding mutations cause isolated or syndromic CHD in humans (human CHD genes), genes for which mouse knockdowns or knockouts are associated with CHD (mouse CHD genes) and the top quarter of expressed genes during heart development (high heart expression genes)[3,4]. To generate the mouse CHD gene set, mammalian phenotype ontology terms of potential relevance to CHD were identified. These were reviewed to remove cardiovascular terms that were not specific to CHD, such as cardiac dilation/hypertrophy, arrhythmias and coronary artery disease[69]. Data on the mouse strains associated with these mammalian phenotype ontology terms were downloaded (http://www.mousemine.org/mousemine). Only single-gene transgenic mutant mouse strains were kept, and these mouse genes were converted to their human orthologs (ftp://ftp.informatics.jax.org/pub/reports/HOM_MouseHumanSequence.rpt).

Multiple hypothesis testing correction for region-based test. The *P* value threshold was determined by correcting for the number of independently tested hypotheses. Because the 184 noncoding features were highly correlated (Supplementary Fig. 1), the number of independent hypothesis tests was set as the number of eigenvectors that explain ≥99% of the variance in the correlations between the features[41]. A *P* value was simulated for all pair-wise correlations between features. The simulated *P* value was equal to the fraction of 10,000 permutations with a more extreme correlation than that of the observed value. The observed value was calculated according to the overlap between DNVs and features. For each permutation, a random feature overlap matrix was generated by treating the observed overlaps as random variables and sampling from a binomial distribution. Eigenvalue decomposition of these *P* values was used to estimate the number of effective tests that explain ≥99% of the variance in the 184 features. For the 184 noncoding cardiac gene regulatory features, this corresponded to 47 independent, effective tests and a Bonferroni *P* value of 1.1×10^{-3} (0.05/47). These 184 features (that is, 47 effective features) were tested in the context of 6 gene sets and were tested on a genome-wide basis, so we corrected for these additional hypotheses. In order to account for testing 6 gene sets and testing genome-wide for 47 effective noncoding features, a final *P* value cut-off of $1.3\times10^{-4}=0.05/(47\times7)$ was used as a significance threshold for all comparisons.

HeartENN. HeartENN encompasses two neural network-based epigenomic effects models: one for human heart chromatin data and one for mouse heart chromatin data. Both models use the same convolutional neural network architecture but predict different genome-wide features (90 for human and 94 for mouse) based on the heart-specific chromatin profiles available for each organism. The models were trained with PyTorch using the Selene library[70].

Training and evaluation data for the genome-wide features (for example, histone marks, transcription factors and DNase I accessibility) included data processed from the Cistrome, ENCODE and Roadmap Epigenomics projects, as well as a published dataset of 36 genome-wide p300/CBP and H3K27ac ChIP–seq profiles from ex vivo cardiac tissue samples in mouse and human across many conditions and developmental stages (Supplementary Table 7)[11–28].

The architecture of the HeartENN models is extended from the DeepSEA[9,33] architecture. In addition to HeartENN models that predict different regulatory features, the main changes are that: (1) the HeartENN architecture contains double the number of convolution layers, (2) the models predict the epigenomic features of the center 50-bp region and use the remaining 95 bp as the surrounding context sequence and (3) the number of kernels used in each convolution has been reduced (see Supplementary Note for details).

DNVs within RefSeq protein-coding exons were not scored with HeartENN (CHD probands, 792 DNVs; CHD-unaffected individuals, 1,749 DNVs); DNVs in noncoding exons were scored.

Accounting for varying HeartENN thresholds. We compared the number of DNVs in CHD probands to those in unaffected individuals with HeartENN scores above varying thresholds. In this context, optimal power for rejecting the null hypothesis that cases and controls have similar rates of relevant HeartENN scores is achieved with the variable threshold test[71]. This was performed by DNV case–control label swapping across all HeartENN cut-offs in 0.05 intervals. For every resample, we randomly assigned case–control status to DNVs with replacement and identified the most significant *P* value at any cut-off. When this null distribution was compared to the most extreme observed *P* value, a resampling *P* value was obtained.

Induced pluripotent stem cell-derived cardiomyocyte differentiation and ATAC–seq. Accessible chromatin regions during cardiomyocyte differentiation were identified by ATAC–seq analysis of isogenic human iPSC–CMs at several points during various states of differentiation.

Cells were differentiated according to previously described methods with small modifications[72]. One million iPSCs were plated in 6-well plates and were maintained in culture for three days. The differentiation process was performed when cells were ~95% confluent. Differentiation was performed using the GSK inhibitor (ChIR 18 μM) and Wnt inhibitor protocol (IWP4 5 μM)[72]. Selection was performed at days 12–15 using glucose-starved media. Cells were collected at days 8, 17 and 30. Cell viability was required to be >80% for cells collected. Cells were observed under a microscope, and for days 17 and 30, cells were only collected if the whole well was beating (wells that only had beating clusters were discarded).

ATAC–seq was performed as described previously[73,74]. In brief, 50,000 cells were collected and lysed to isolate the nuclei. The nuclei were treated with Tn5 transposase (Nextera DNA Sample Prep Kit, Illumina) and DNA was isolated. Fragmented DNA was then amplified using barcoded PCR primers and libraries were pooled. ATAC libraries were visualized on the tape station for characteristic nucleosome patterning before sequencing. Pooled libraries were then sequenced (Illumina Next-seq) to a depth of 100 million reads per sample. Reads were aligned to the hg19 reference genome using BWA-MEM and peaks were called using HOMERv4.9 (ref. [75]). Functional analysis of ATAC–seq peaks was performed using ChIPseeker (v.1.14.1)[76]. De novo motif enrichment was performed using HOMERv4.9. Differential peaks were identified using HOMERv4.9. Libraries that contained an excess of mitochondrial DNA (>15% for iPSC–CMs) were removed. Each replicate was analyzed individually ($n = 3$–4 per time point) and compared to other replicates at the same time point, and data were also visualized in the IGV/University of California Santa Cruz Genome Browser. Comparison of any two replicates resulted in approximately 85–95% peak overlap between replicates.

Enrichment for genes with burden of de novo variants in associated fetal cardiac enhancers. Cardiac enhancer elements were identified by H3K27ac peaks from human cardiac tissue[77]. Enhancer peaks were assigned to the closest RefSeq TSS and intersected with ATAC–seq peaks from day 8 or day 17 (Induced pluripotent stem cell-derived cardiomyocyte differentiation and ATAC–seq). The likelihood of multiple genes having DNV enrichment was assessed by randomly permuting the 7,378 total DNVs associated with the prioritized human fetal heart enhancers to case or control status with the same 2,218:5,160 ratio. The number of genes with enrichment $P < 0.05$ in either cohort was calculated using a two-sided Fisher's exact test.

Massively parallel reporter assays. The effect of CHD noncoding DNVs on enhancer activity was assessed by MPRAs[40], using constructs with longer sequences so as to assess those residing in broad ATAC peaks identified in D17 iPSC–CM peaks. DNVs were selected for study using the following criteria: HeartENN score ≥ 0.1 and with a prioritized human fetal heart enhancer (8 of 9 tested); HeartENN score ≥ 0.5 (11 of 22 tested); prioritized human fetal heart enhancer for which the associated gene was highly expressed in the developing heart (mouse E14.5 expression rank >75th percentile) and highly constrained (pLi > 0.8) (9 of 24 tested); and HeartENN score ≥ 0.1 and within a strong iPSC–CM day 8 or day 17 ATAC–seq peak as well as an overlapping human fetal H3K27ac peak (11 of 24 tested). Of note, most of the DNVs that met those criteria and that were not tested either contained a restriction site that would have prevented cloning of the full-length sequence or had repetitive sequences that were problematic for synthesis.

Gene fragments of 300–1,600 bp in length that harbored reference and variant alleles were synthesized by Twist Bioscience. Each fragment was separately PCR amplified and SfiI restriction enzyme sites were incorporated. After the fragments were cleaned with AmpureXP beads, equimolar amounts of pooled constructs were combined. To minimize occurrence of the restriction enzyme site in the enhancer sequences, SalI was substituted for XbaI when the inserts were cloned and to accommodate this change, the SalI site downstream of the poly(A) signal in the pMPRA1 plasmid (Addgene 49349) was mutated, using MfeI and BbsI sites in proximity. Modified MPRA plasmid sequences were verified using Sanger sequencing.

Gene fragments were cloned using the published MPRA protocol[40]. In short, the pooled enhancer fragments were digested with SfiI and ligated to the modified and digested pMPRA1 backbone with T4 DNA ligase. Plasmids were transformed into DH5α electrocompetent *Escherichia coli* cells and plasmid DNA was isolated using a Qiagen Maxiprep kit. Isolated plasmid DNA was digested with SalI and KpnI in the presence of shrimp alkaline phosphatase. Promoter and luciferase sequences isolated from pMPRAdonor2 (Addgene 49353) were then cloned into the intermediate plasmid. The final plasmid library was washed and concentrated with 70% ethanol, air dried and redissolved in sterile water.

iPSCs were cultured under standard condition using the culture medium mTesr. iPSCs were differentiated into CMs using the standard protocol[78], and iPSC–CMs were selectively enriched using glucose starvation for 4 d. iPSC–CMs were replated into monolayers with 10× TrypLE cell dissociation reagent. After replating, healthy cells that were vigorously beating were used for library transfection using Lipofectamine 3000 according to the manufacturer's instructions. Total RNA was harvested with Trizol 48 h after transfection, and genomic DNA was removed with DNase I. cDNAs were synthesized using the SuperScript III First Strand Synthesis kit with oligo(dT) according to the manufacturer's instructions. MPRA barcodes were amplified from cDNAs and plasmids using the Tagseq primers.

Sequencing reads that contained the correct plasmid sequences were selected from raw reads. Barcode sequences were then matched, counted and normalized to the total number of barcode reads in the sequencing run.

Every variant in the 'HeartENN ≥ 0.1 + FHP' group was replicated using four independent plasmid libraries; variants in the remaining 3 groups were replicated using 3 independent plasmid libraries. Libraries 1, 2 and 4 were transfected on differentiation day 17, while the third was transfected on day 37. Each plasmid library experiment was repeated in four or five wells. Together, this resulted in 12–20 expression measurements per mutant and wild-type variant with an extremely robust set of replicates incorporating different wells, plasmid libraries and time points.

RNA-binding-protein eCLIP binding data. Raw eCLIP binding data for the 160 available RBPs were obtained from ENCODE[15]. Peaks were called from replicates using the CLIP Took Kit[79] and were further processed[80] into a narrower, higher confidence set of binding regions for each RBP. All peaks were then given 50-bp padding on both sides to expand the genomic coverage and increase the number of variants associated with each RBP.

Analysis of disruption of post-transcriptional regulation. Five groups of annotations were defined to investigate post-transcriptional regulation through disruption of RBP binding, as follows: (1) 3 variant types (SNV, indel and all); (2) 3 region types (TSS ± 20 kb region anchor, 3′UTR region anchor defined as (transcription end site (TES) – 5 kb and TES + 20 kb) and no region restriction); (3) 1 RBP category (union of eCLIP peaks from 160 RBPs, padded on both sides with 50 bp); (4) 2 gene sets (unconstrained or pLI > 0.5 constraint on nearest gene) and (5) histone mark annotations for actively transcribed regions in relevant proxy tissues, specifically H3K36me3 in 8 human embryonic stem cell lines—ES-I3 stem cells (NIH Roadmap Epigenomics numeric identifier E001), ES-WA7 stem cells (E002), H1 stem cells (E003), H9 stem cells (E008), HUES48 stem cells (E014), HUES6 stem cells (E015), HUES64 stem cells (E016) and ES-UCSF4 stem cells (E024)—plus human fetal heart tissue (E083).

Histone modification peaks were downloaded as broadPeak files, originally determined from Roadmap Epigenomics ChIP–seq data[25]. Raw broadPeaks were preprocessed as follows to include the majority of the area between the 5′ and 3′ UTRs for transcribed genes and to reduce noise in the identification of actively transcribed regions in proxy tissues: gaps under 1 kb between histone peaks within this region were filled in, which resulted in a slightly improved signal throughout for genes with many nearby peaks.

When one annotation from each group was picked, this resulted in 162 possible combinations. These annotation categories were considered in the combination-wide association test and provided 105 independent tests, giving 4.76×10^{-4} as the strict Bonferroni threshold. Two-sided Fisher's exact tests were used to obtain ORs and associated *P* values for all test combinations. DNVs within RefSeq protein-coding exons were excluded.

Attributable risk calculation. The fraction of CHD cases that are attributable to noncoding DNVs was calculated by determining the excess fraction of DNVs in cases compared to those in controls (equation (1)); we then assumed at most one contributory DNV per proband to calculate the attributable fraction (equation (2)). This AR was calculated for HeartENN-damaging DNVs at successively stringent thresholds, DNVs within prioritized human fetal heart enhancers in multiple gene sets, DNVs shared between these results and DNVs implicated in the top RBP enrichment. The AR is cumulative across methods (after subtracting out the contribution of shared DNVs) and represents an estimate that should be refined in future studies.

$$AR_{DNV} = \left(\frac{DNV_{cases,candidate}}{DNV_{cases,total}} - \frac{DNV_{controls,candidate}}{DNV_{controls,total}}\right) \quad (1)$$

$$AR_{cases} = \frac{AR_{DNV} \times DNV_{cases,total}}{n_{cases}} \quad (2)$$

Statistics. All burden tests were calculated using two-sided Fisher's exact tests with base values set to the total number of DNVs in cases or controls. Parental age is accounted for by using the total number of DNVs, instead of the number of trios, as a baseline. The significance threshold was $P < 0.05$, adjusted for multiple testing within each hypothesis space as specified in the preceding Methods.

Reporting Summary. Further information on research design is available in the Nature Research Reporting Summary linked to this article.

Data availability

Whole-genome sequencing data are deposited in the database of Genotypes and Phenotypes (dbGaP) under accession numbers phs001194.v2.p2 and phs001138.v2.p2.

Code availability

Documentation, links, and availability of source code and select supplementary data are detailed at https://github.com/frichter/wgs_chd_analysis. The DNV identification pipeline is available at https://github.com/ShenLab/igv-classifier and https://github.com/frichter/dnv_pipeline. The HeartENN algorithmic framework is available at https://github.com/FunctionLab/selene/archive/0.4.8.tar.gz. HeartENN model weights and scripts for burden tests are available at https://github.com/frichter/wgs_chd_analysis. All source code is distributed under the Massachusetts Institute of Technology license.

References

60. Li, H. & Durbin, R. Fast and accurate short read alignment with Burrows–Wheeler transform. *Bioinformatics* **25**, 1754–1760 (2009).
61. McKenna, A. et al. The Genome Analysis Toolkit: a MapReduce framework for analyzing next-generation DNA sequencing data. *Genome Res.* **20**, 1297–1303 (2010).
62. DePristo, M. A. et al. A framework for variation discovery and genotyping using next-generation DNA sequencing data. *Nat. Genet.* **43**, 491–498 (2011).
63. Van der Auwera, G. et al. From FastQ data to high-confidence variant calls: the genome analysis toolkit best practices pipeline. *Curr. Protoc. Bioinformatics* **43**, 11.10.1–11.10.33 (2013).
64. Kim, B.-Y., Park, J. H., Jo, H.-Y., Koo, S. K. & Park, M.-H. Optimized detection of insertions/deletions (INDELs) in whole-exome sequencing data. *PLoS One* **12**, e0182272 (2017).
65. Bailey, J. A., Yavor, A. M., Massa, H. F., Trask, B. J. & Eichler, E. E. Segmental duplications: organization and impact within the current human genome project assembly. *Genome Res.* **11**, 1005–1017 (2001).
66. Derrien, T. et al. Fast computation and applications of genome mappability. *PLoS One* **7**, e30377 (2012).
67. Li, H. Toward better understanding of artifacts in variant calling from high-coverage samples. *Bioinformatics* **30**, 2843–2851 (2014).
68. Ostrander, B. E. P. et al. Whole-genome analysis for effective clinical diagnosis and gene discovery in early infantile epileptic encephalopathy. *NPJ Genom. Med.* **3**, 22 (2018).
69. Blake, J. A. et al. Mouse Genome Database (MGD)-2017: community knowledge resource for the laboratory mouse. *Nucleic Acids Res.* **45**, D723–D729 (2017).
70. Chen, K. M., Cofer, E. M., Zhou, J. & Troyanskaya, O. G. et al. Selene: a PyTorch-based deep learning library for sequence data. *Nat. Methods* **16**, 315–318 (2019).
71. Price, A. L. et al. Pooled association tests for rare variants in exon-resequencing studies. *Am. J. Hum. Genet.* **86**, 832–838 (2010).
72. Lian, X. et al. Directed cardiomyocyte differentiation from human pluripotent stem cells by modulating Wnt/β-catenin signaling under fully defined conditions. *Nat. Protoc.* **8**, 162–175 (2013).
73. Buenrostro, J. D., Wu, B., Chang, H. Y. & Greenleaf, W. J. ATAC–seq: a method for assaying chromatin accessibility genome-wide. *Curr. Protoc. Mol. Biol.* **109**, 21.29.1–21.29.9 (2015).
74. Corces, M. R. et al. An improved ATAC–seq protocol reduces background and enables interrogation of frozen tissues. *Nat. Methods* **14**, 959–962 (2017).
75. Heinz, S. et al. Simple combinations of lineage-determining transcription factors prime *cis*-regulatory elements required for macrophage and B cell identities. *Mol. Cell* **38**, 576–589 (2010).
76. Yu, G., Wang, L.-G. & He, Q.-Y. ChIPseeker: an R/Bioconductor package for ChIP peak annotation, comparison and visualization. *Bioinformatics* **31**, 2382–2383 (2015).
77. Spurrell, C. H. et al. Genome-wide fetalization of enhancer architecture in heart disease. Preprint at *bioRxiv* https://doi.org/10.1101/591362 (2019).
78. Sharma, A., Toepfer, C. N., Schmid, M., Garfinkel, A. C. & Seidman, C. E. Differentiation and contractile analysis of GFP-sarcomere reporter hiPSC-cardiomyocytes. *Curr. Protoc. Hum. Genet.* **96**, 21.12.1–21.12.12 (2018).
79. Shah, A., Qian, Y., Weyn-Vanhentenryck, S. M. & Zhang, C. CLIP Tool Kit (CTK): a flexible and robust pipeline to analyze CLIP sequencing data. *Bioinformatics* **33**, 566–567 (2017).
80. Feng, H. et al. Modeling RNA-binding protein specificity in vivo by precisely registering protein-RNA crosslink sites. *Mol. Cell* **74**, 1189–1204.e6 (2019).

Acknowledgements

We are enormously grateful to the patients and families who participated in this research. We thank the following for patient recruitment: A. Julian, M. MacNeal, Y. Mendez, T. Mendiz-Ramdeen and C. Mintz (Icahn School of Medicine at Mount Sinai); N. Cross (Yale School of Medicine); J. Ellashek and N. Tran (Children's Hospital of Los Angeles); B. McDonough, J. Geva and M. Borensztein (Harvard Medical School); K. Flack, L. Panesar and N. Taylor (University College London); E. Taillie (University of Rochester School of Medicine and Dentistry); S. Edman, J. Garbarini, J. Tusi and S. Woyciechowski (Children's Hospital of Philadelphia); D. Awad, C. Breton, K. Celia, C. Duarte, D. Etwaru, N. Fishman, E. Griffin, M. Kaspakoval, J. Kline, R. Korsin, A. Lanz, E. Marquez, D. Queen, A. Rodriguez, J. Rose, J. K. Sond, D. Warburton, A. Wilpers and R. Yee (Columbia Medical School); D. Gruber (Cohen Children's Medical Center, Northwell Health). These data were generated by the PCGC, under the auspices of the Bench to Bassinet Program (https://benchtobassinet.com) of the NHLBI. The results analyzed and published here are based in part on data generated by Gabriella Miller Kids First Pediatric Research Program projects phs001138.v1.p2/phs001194.v1.p2, and were accessed from the Kids First Data Resource Portal (https://kidsfirstdrc.org/) and/or dbGaP (www.ncbi.nlm.nih.gov/gap). This manuscript was prepared in collaboration with investigators of the PCGC and has been reviewed and/or approved by the PCGC. PCGC investigators are listed at https://benchtobassinet.com/?page_id=119. This work was supported in part through the computational resources and staff expertise provided by Scientific Computing at the Icahn School of Medicine at Mount Sinai. We are grateful to all of the families at the participating Simons Simplex Collection (SSC) sites, as well as the principal investigators (A. Beaudet, R. Bernier, J. Constantino, E. Cook, E. Fombonne, D. Geschwind, R. Goin-Kochel, E. Hanson, D. Grice, A. Klin, D. Ledbetter, C. Lord, C. Martin, D. Martin, R. Maxim, J. Miles, O. Ousley, K. Pelphrey, B. Peterson, J. Piggot, C. Saulnier, M. State, W. Stone, J. Sutcliffe, C. Walsh, Z. Warren and E. Wijsman). We appreciate the access obtained to phenotypic and/or genetic data on SFARI Base. Approved researchers can obtain the SSC population dataset described in this study (https://www.sfari.org/resource/simons-simplex-collection) by applying at https://base.sfari.org. This work was supported by the Mount Sinai Medical Scientist Training Program (5T32GM007280 to F.R.), National Institute of Dental and Craniofacial Research Interdisciplinary Training in Systems and Developmental Biology and Birth Defects (T32HD075735 to F.R.), Harvard Medical School Epigenetic and Gene Dynamics Award (S.U.M. and C.E.S.), American Heart Association Post-Doctoral Fellowship (S.U.M.), and Howard Hughes Medical Institute (C.E.S.). Research conducted at the E.O. Lawrence Berkeley National Laboratory was supported by National Institutes of Health (NIH) grants (UM1HL098166 and R24HL123879) and performed under Department of Energy Contract DE-AC02-05CH11231, University of California. O.T. is a CIFAR fellow and this work was partially supported by NIH grant R01GM071966. The PCGC program is funded by the NHLBI, NIH, US Department of Health and Human Services through grants UM1HL128711, UM1HL098162, UM1HL098147, UM1HL098123, UM1HL128761 and U01HL131003. The PCGC Kids First study includes data sequenced by the Broad Institute (U24 HD090743-01).

Author contributions

F.R., S.U.M., S.W.K., A.K., L.K.W., K.M.C., J.R.K., O.G.T., D.E.D., Y.S., J.G.S., C.E.S. and B.D.G. conceived and designed the experiments/analyses. J.R.K., J.W.N., A.G., E.G., M.B., R.K., G.A.P., D.B., W.K.C., D.S., M.T.-F., J.G.S., C.E.S. and B.D.G. contributed to cohort ascertainment, phenotypic characterization and recruitment. F.R., S.U.M., A.K., H.Q., N.P., S.R.D., M.P., J.H., J.M.G., K.B.M., M.V., A.F., G.M., W.K.C., Y.S., J.G.S., C.E.S. and B.D.G. contributed to whole-genome sequencing production, validation and analysis. F.R., S.U.M., A.K., K.M.C., H.Q., E.E.S., O.G.T., Y.S., J.G.S., C.E.S. and B.D.G. contributed to statistical analyses. F.R., K.M.C., J.Z., O.G.T. and B.D.G. developed the HeartENN model. S.U.M., S.W.K., L.K.W., D.E.D., J.G.S. and C.E.S. generated and analyzed fetal heart and iPSC data. F.R., S.U.M., S.W.K., A.K., L.K.W., K.M.C., Y.S., J.G.S., C.E.S. and B.D.G. wrote and reviewed the manuscript. All authors read and approved the manuscript.

Competing interests

The authors declare no competing interests.

Additional information

Extended data is available for this paper at https://doi.org/10.1038/s41588-020-0652-z.

Supplementary information is available for this paper at https://doi.org/10.1038/s41588-020-0652-z.

Correspondence and requests for materials should be addressed to B.D.G.

Reprints and permissions information is available at www.nature.com/reprints.

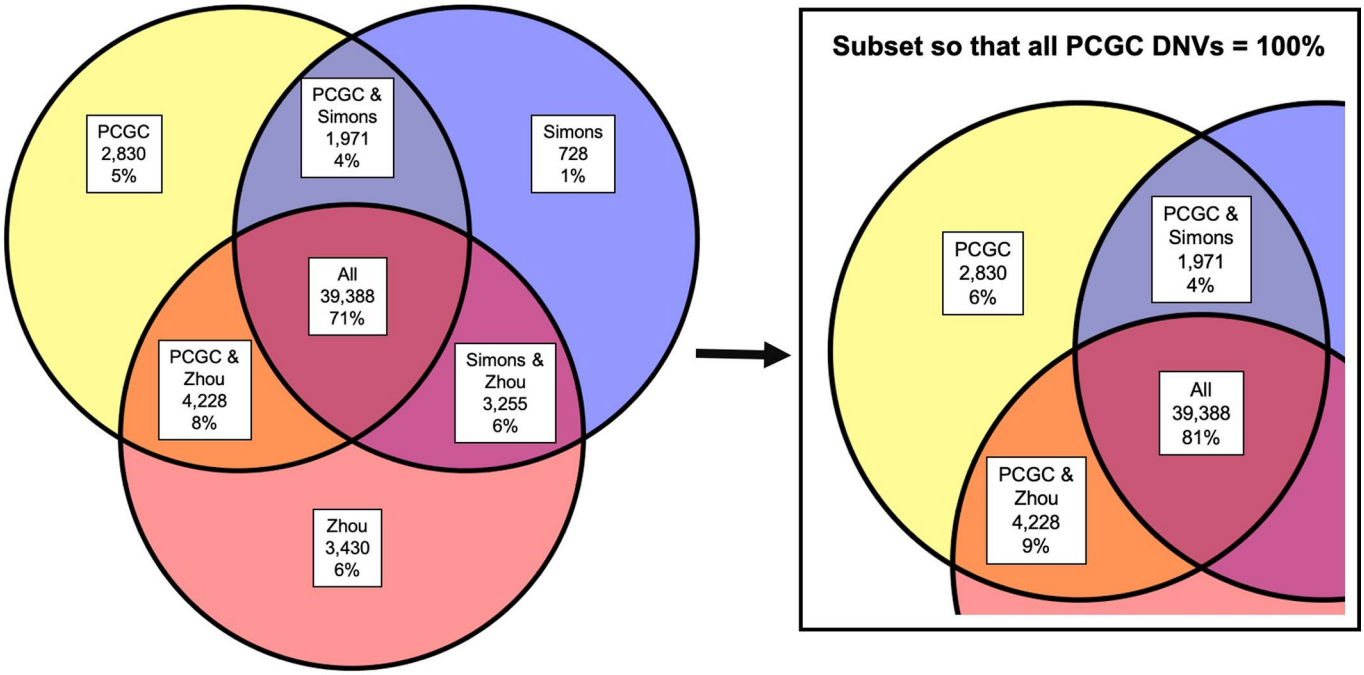

Extended Data Fig. 1 | Other pipelines identified 94% of DNVs in control trios. Overlaps with DNVs identified in 1,470 control trios with two other pipelines[9,10]. Of note, a third analysis of these trios did not include *de novo* calls[42]. For consistency with other pipelines, only SNVs were included and variants in LCRs, blacklists, segmental duplications, and repeats were excluded. Together, 94% of *de novo* SNVs were called by at least one other pipeline.

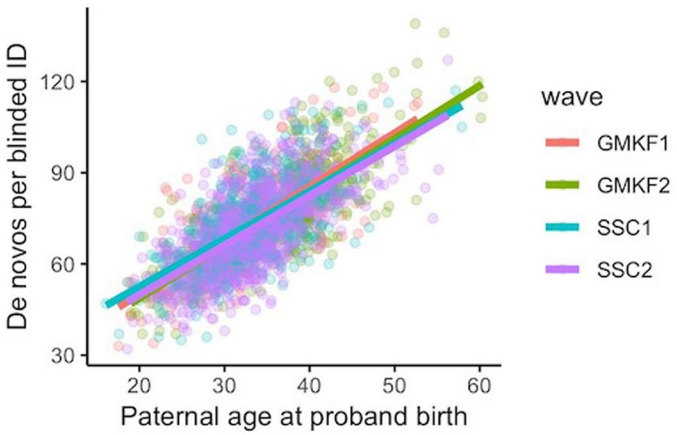

	Coefficient	Cases (N=763)		Controls (N=1627)	
		β	*P*	β	*P*
All	**Paternal age**	1.4	$5x10^{-54}$	1.4	$6x10^{-86}$
	Maternal age	0.5	$2x10^{-5}$	0.4	$3x10^{-8}$
	Intercept	11.8	$8x10^{-8}$	14.4	$5x10^{-17}$
SNVs	**Paternal age**	1.4	$2x10^{-53}$	1.3	$1x10^{-86}$
	Maternal age	0.4	$2x10^{-5}$	0.4	$5x10^{-8}$
	Intercept	9.5	$5x10^{-6}$	12.4	$3x10^{-14}$
Indels	**Paternal age**	0.07	$2x10^{-4}$	0.05	$3x10^{-4}$
	Maternal age	0.01	0.6	0.03	0.1
	Intercept	2.2	$4x10^{-6}$	2.0	$3x10^{-7}$

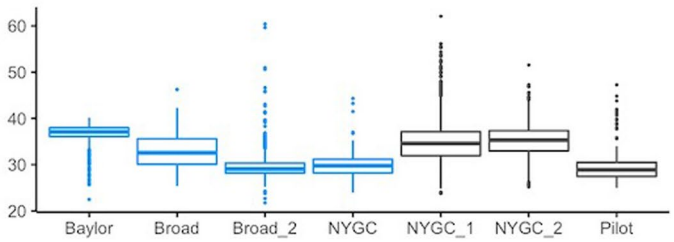

Mean coverage
ANOVA F-statistic P $<10^{-16}$
Kruskal-Wallis P $<10^{-16}$

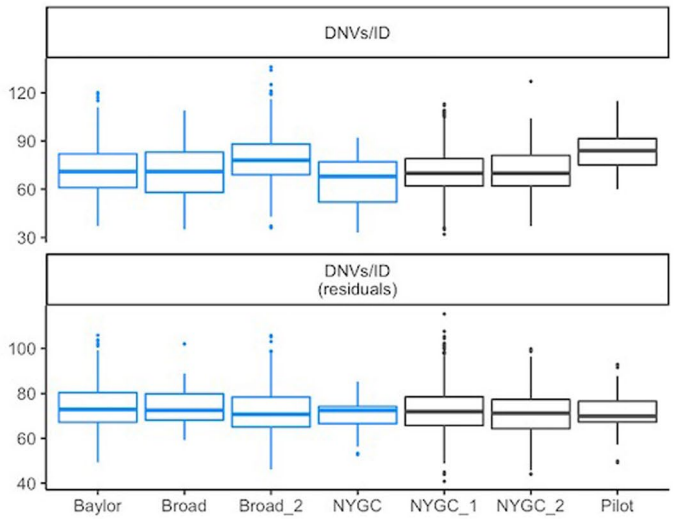

***De novo* variants per ID**
ANOVA F-statistic P $<10^{-16}$
Kruskal-Wallis P $<10^{-16}$

***De novo* variants per ID after regressing out parental age**
ANOVA F-statistic P=0.025
- Tukey post-hoc only P<0.05 is NYGC2 vs Baylor (P=0.012)

Kruskal-Wallis P=0.066
- No Dunn post-hoc P<0.05 (NYGC2 vs Baylor P=0.051)

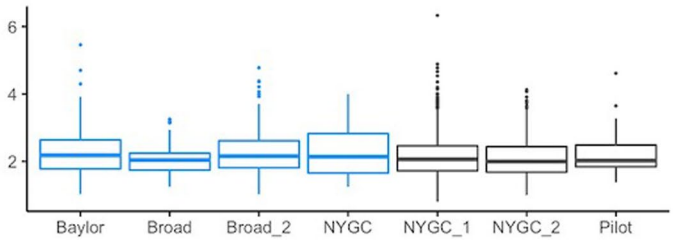

***De novo* Ts/Tv ratio**
ANOVA F-statistic P=0.0013
- P<0.05 for NYGC 2 vs Baylor (P=0.0046) and NYGC 2 vs Broad 2 (P=0.0050). Other *P* range 0.17-1.0

Kruskal-Wallis P=$6.3x10^{-4}$
- P<0.05 for NYGC 2 vs Baylor (P=0.0025) and NYGC 2 vs Broad 2 (P=0.0024).

Extended Data Fig. 2 | Correlation between parental age at proband birth and DNVs/trio. Multiple linear regression ($\beta_{paternal\_age}x + \beta_{maternal\_age}x + \beta_{intercept} + \varepsilon$) was fitted on 763 CHD and 1,611 unaffected individuals to calculate the associations between paternal and maternal age for SNVs, indels, and combined. Regression coefficients and *P*-values are shown, uncorrected for multiple hypotheses. Sequencing metric comparisons between the centers, colored by cases ($n = 763$) and controls ($n = 1{,}611$), found moderate bias in DNV quantity, so the background statistical parameter throughout the manuscript is total number of DNVs. Box plots show medians and interquartile ranges.

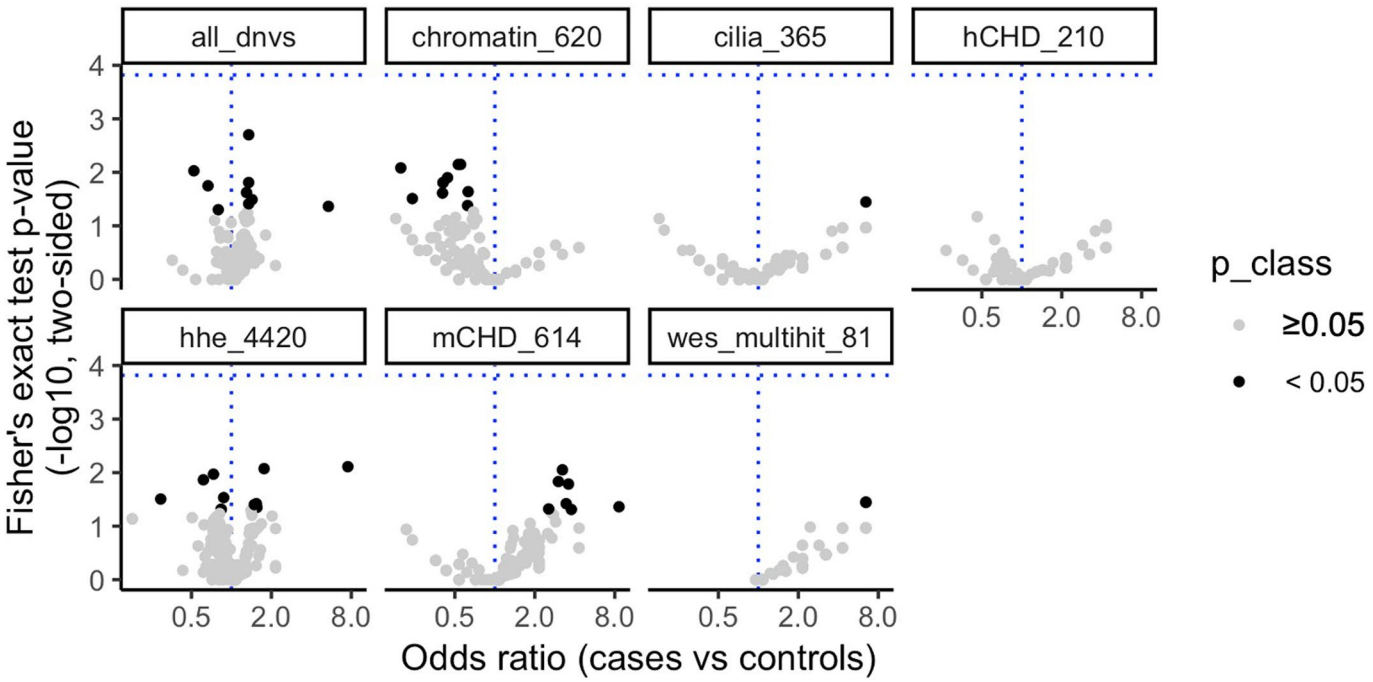

Extended Data Fig. 3 | *De novo* variant (DNV) CHD-unaffected burden. The number of DNVs in 184 noncoding annotations (points) genome-wide and within 10 kb of TSSs for 6 gene sets (facets) was counted in CHD ($n = 749$) and Simons unaffected ($n = 1{,}611$) individuals. The P value threshold (1.5×10^{-4}, horizontal blue line) is 0.05 divided by the product of the number of effective annotations ($n = 47$) and number of gene sets ($n = 7$). The P value (y-axis) was calculated with a two-sided Fisher's exact test, the odds ratio (x-axis) was $DNVs_{annotation,CHD}/DNVs_{total,CHD}$ vs. $DNVs_{annotation,unaffected}/DNVs_{total,\ unaffected}$. No annotations surpassed the P value threshold. CHD, congenital heart disease; HHE, high heart expression.

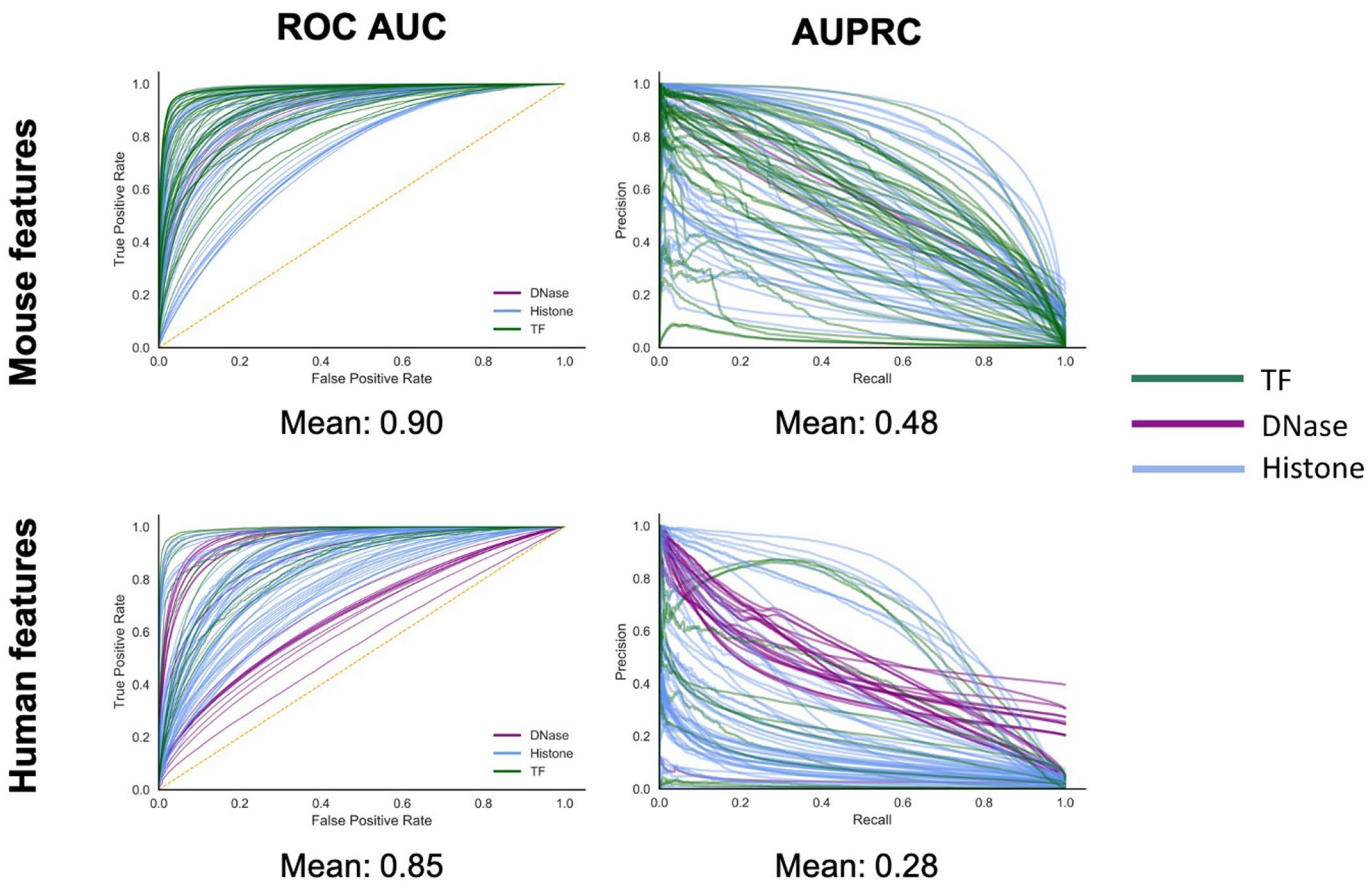

Extended Data Fig. 4 | HeartENN performance was comparable to DeepSEA. HearENN ROC AUC mean = 0.93 and AUPRC mean = 0.34. ROC AUC, receiver operator characteristics area under the curve; AUPRC, area under the precision recall curve.

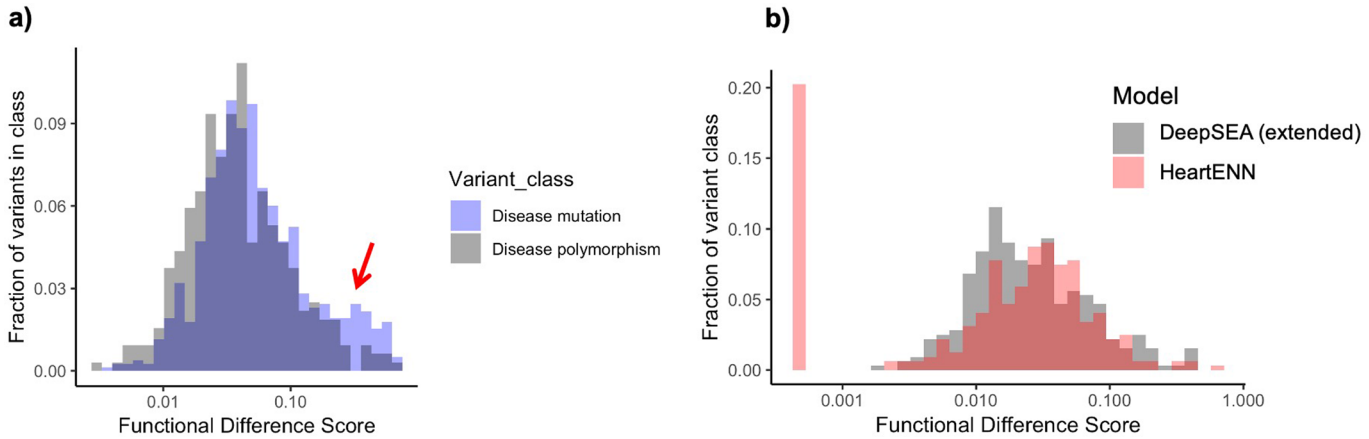

Extended Data Fig. 5 | Determining an absolute functional difference score range. a, Comparison of HGMD disease mutations (blue, $n = 1{,}564$) and polymorphism (gray, $n = 642$) DeepSEA absolute functional difference scores at varying functional cut-offs illustrates a similar distribution and functionally impactful range ≥0.1 (arrow) for disease mutations. No statistical significance testing was performed. **b**, The similarity of null distributions for DeepSEA (gray, downsampled to 184 features) and HeartENN (heart) HGMD polymorphism scores suggested that the DeepSEA functional score range was also applicable to HeartENN (gray and red $n = 642$). Scores of 0 set off to left (as 10^{-4}).

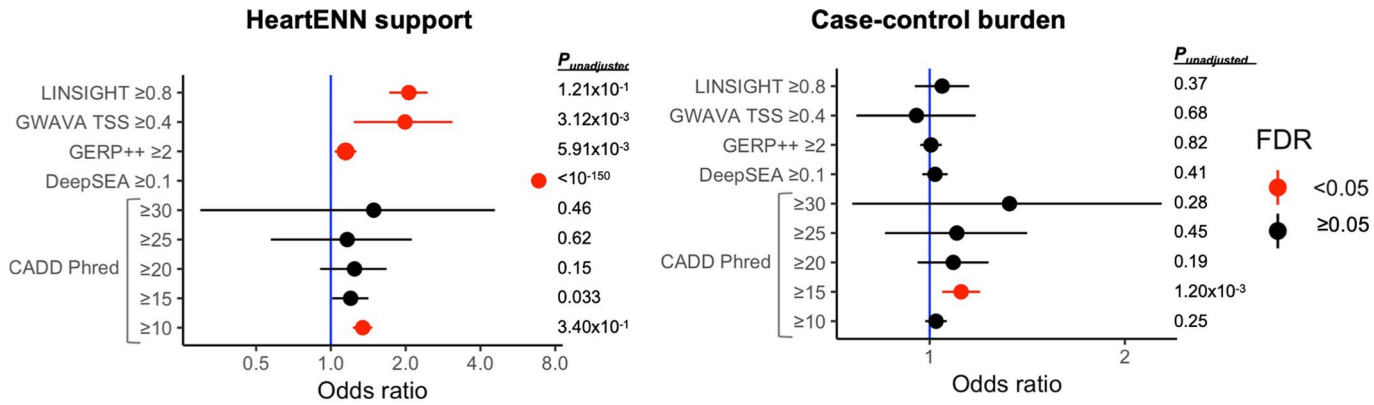

Extended Data Fig. 6 | Support for HeartENN ≥ 0.1 functional ranking. For all DNVs ($n = 170{,}171$), overlap between HeartENN ≥0.1 ($n = 6{,}415$) and other noncoding scores was assessed with a two-sided Fisher's exact test (left panel). Case–control burden for these other noncoding scores (right panel) was statistically significant for CADD ≥15 ($P_{Bonferroni} = 0.019$) with a two-sided Fisher's exact test (cases $n = 56{,}164$ and controls $n = 114{,}065$). For both panels, unadjusted *P*-values are tabulated, and red indicates a Benjamini-Hochberg-adjusted *P* value false discovery rate (FDR) < 0.05.

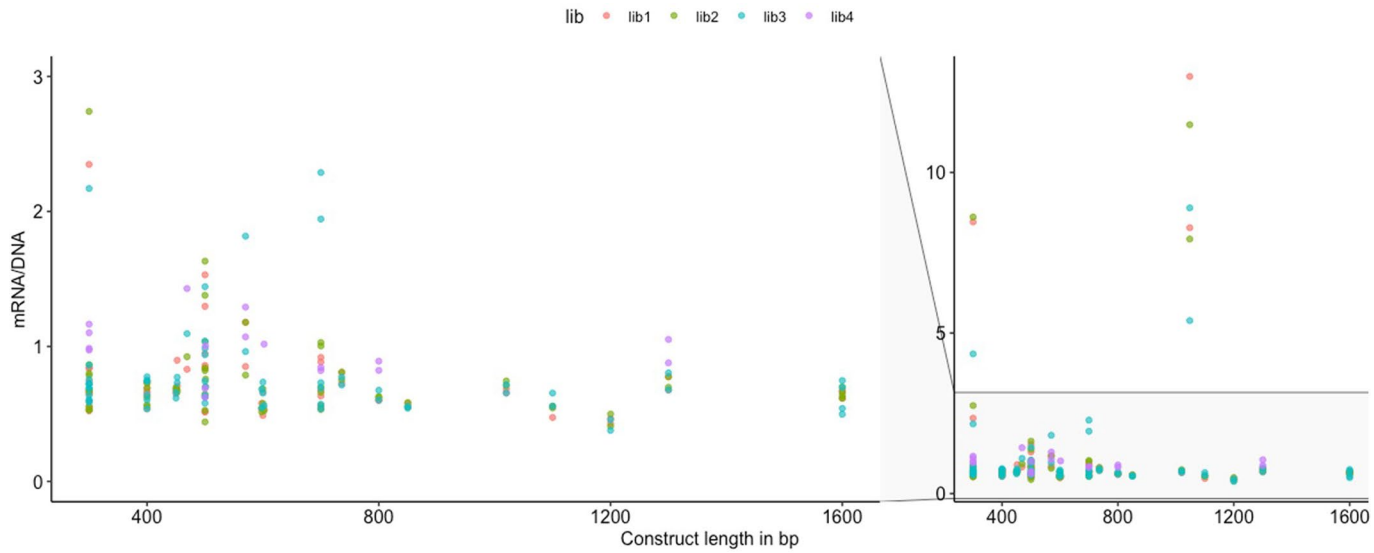

Extended Data Fig. 7 | Relationship between sequence length inserted into the pMRPA1 plasmid and the transcript reads/plasmid copies in MPRAs. The length of the sequences inserted into the pMPRA1 plasmid (*x*-axis) ranged from 300 to 1,600 bp. After transfection of four libraries (color coded as per key) into the iPSC–CMs, the resulting ratios of transcript reads (mRNA) per plasmid copies (DNA) are graphed on the *y*-axis, showing no systematic relationship between insert length and transcriptional level.

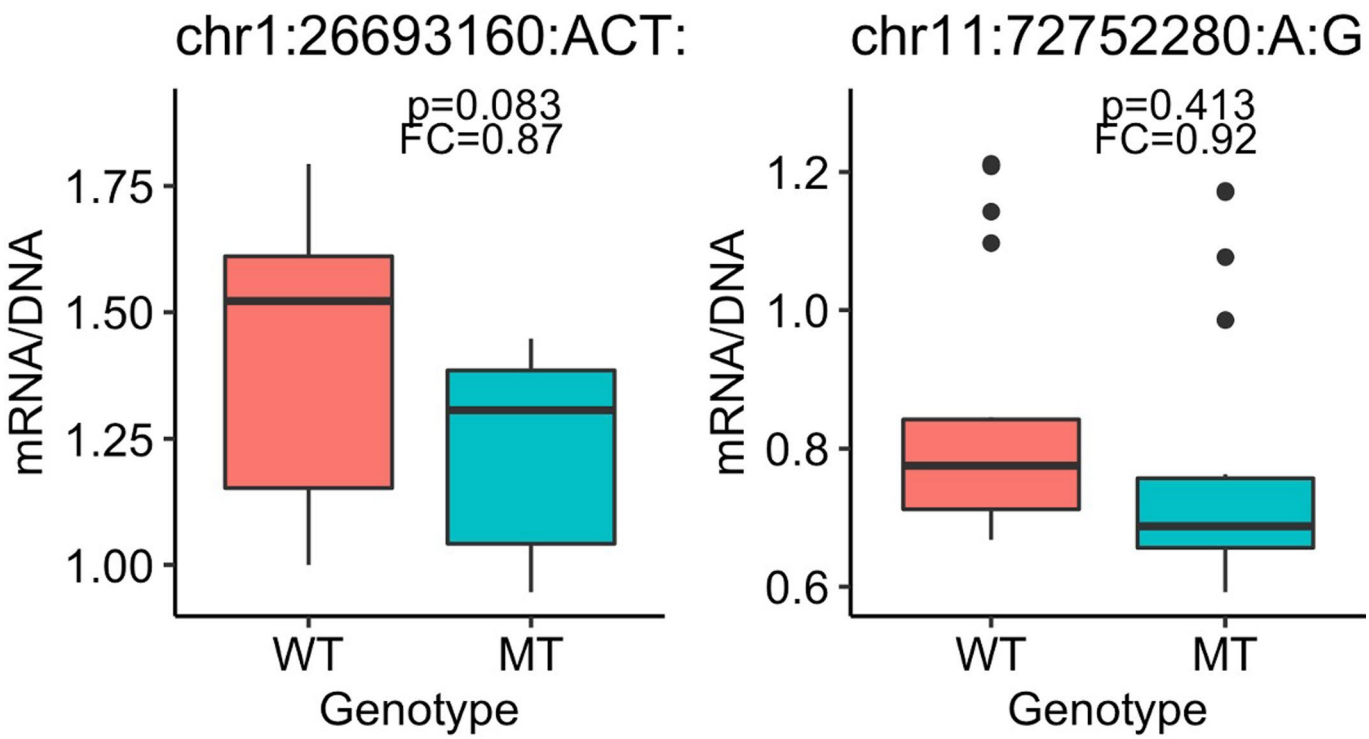

Extended Data Fig. 8 | DNVs with a trend towards decreased expression by MPRA assay. Box plots for two DNVs for which two MPRA replicates were significantly different but overall statistical significance across all replicates was not attained. Boxplots show the median fold change (FC), first and third quartiles (lower and upper hinges), and range of values (whiskers and outlying points). Statistical significance was assessed with two-sided *t*-test Benjamini-Hochberg-adjusted *P*-values. Each boxplot has at least 3 independent experiments with 4 technical replicates each.

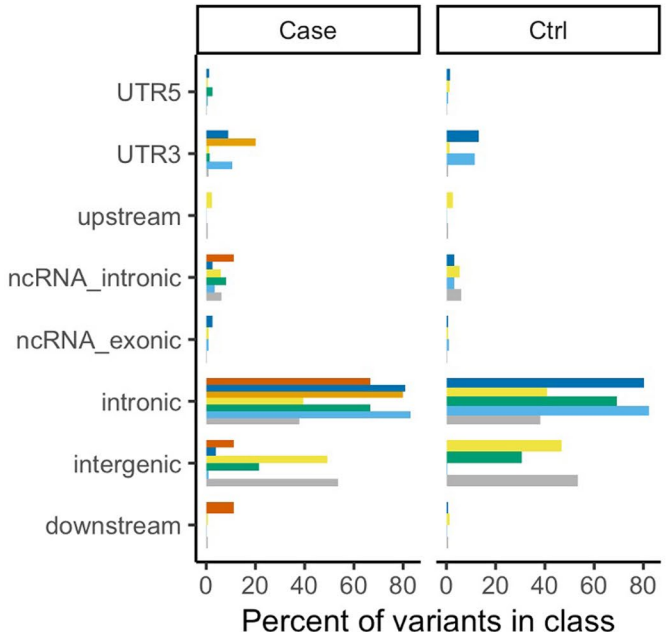

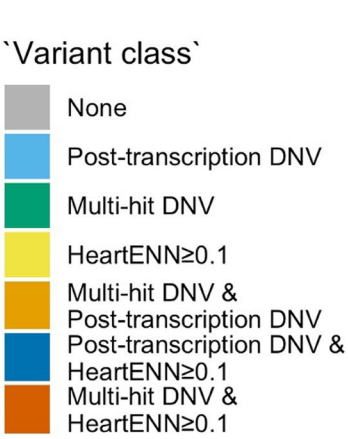

CHD	Unaffected
52,199	106,957
1,584	2,918
81	13
2,151	4,055
10	0
78	122
9	0

Extended Data Fig. 9 | Fraction of DNVs in each of the canonical variant classes. The fraction was calculated separately within CHD and unaffected subjects for each of the three methods (including overlaps) and the total number of variants in each group (right table).

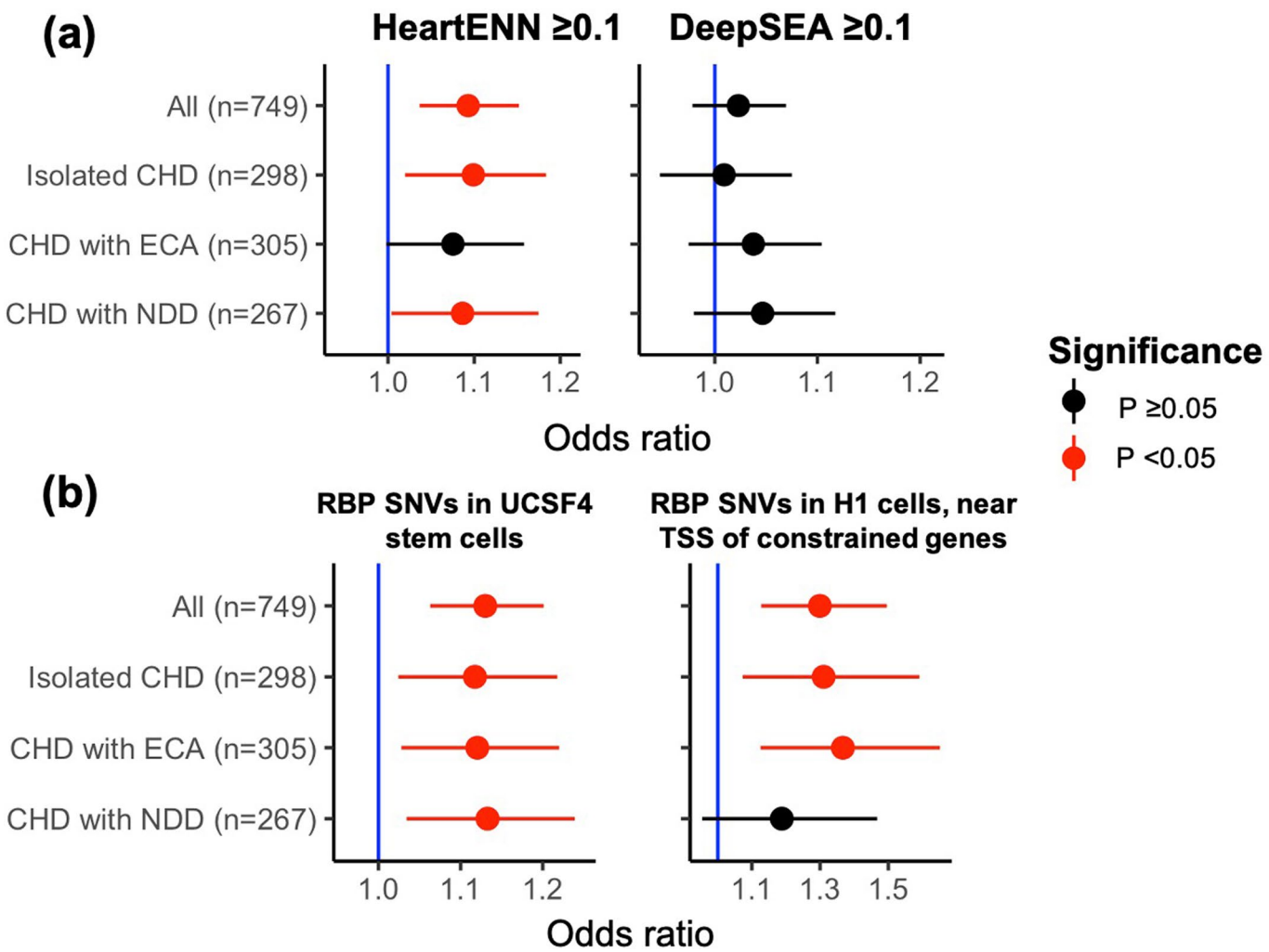

Extended Data Fig. 10 | DNV enrichment in phenotype subgroups. a, Enrichment of DNVs with predicted functional impacts (score ≥0.1) for HeartENN (left) and DeepSEA (right) within phenotype subgroups. **b**, Enrichment of *de novo* SNVs with H3K36me3 marks implicated in RNA-binding protein disruption in different subgroups for the most significant (left) and highest effect size (right) hits. Both **a** and **b** were performed with a two-sided Fisher's exact test (unadjusted *P*-values and 95% C.I.s shown) comparing the fraction of DNVs in each subgroup (HeartENN ≥ 0.1, DeepSEA ≥ 0.1, etc.) to the same control cohort. For HeartENN, there were $n = 4{,}177$ control DNVs with HeartENN ≥ 0.1 and $n = 109{,}888$ control DNVs with HeartENN < 0.1. NDD, neurodevelopmental disorder; ECA, extracardiac anomaly.

nature research

Corresponding author(s): Bruce D. Gelb

Last updated by author(s): Apr 8, 2019

Reporting Summary

Nature Research wishes to improve the reproducibility of the work that we publish. This form provides structure for consistency and transparency in reporting. For further information on Nature Research policies, see Authors & Referees and the Editorial Policy Checklist.

Statistics

For all statistical analyses, confirm that the following items are present in the figure legend, table legend, main text, or Methods section.

n/a	Confirmed	
☐	☒	The exact sample size (*n*) for each experimental group/condition, given as a discrete number and unit of measurement
☐	☒	A statement on whether measurements were taken from distinct samples or whether the same sample was measured repeatedly
☐	☒	The statistical test(s) used AND whether they are one- or two-sided *Only common tests should be described solely by name; describe more complex techniques in the Methods section.*
☐	☒	A description of all covariates tested
☐	☒	A description of any assumptions or corrections, such as tests of normality and adjustment for multiple comparisons
☐	☒	A full description of the statistical parameters including central tendency (e.g. means) or other basic estimates (e.g. regression coefficient) AND variation (e.g. standard deviation) or associated estimates of uncertainty (e.g. confidence intervals)
☐	☒	For null hypothesis testing, the test statistic (e.g. *F*, *t*, *r*) with confidence intervals, effect sizes, degrees of freedom and *P* value noted *Give P values as exact values whenever suitable.*
☒	☐	For Bayesian analysis, information on the choice of priors and Markov chain Monte Carlo settings
☒	☐	For hierarchical and complex designs, identification of the appropriate level for tests and full reporting of outcomes
☐	☒	Estimates of effect sizes (e.g. Cohen's *d*, Pearson's *r*), indicating how they were calculated

Our web collection on statistics for biologists contains articles on many of the points above.

Software and code

Policy information about availability of computer code

Data collection	REDCap and HeartsMart (https://pcgc.research.cchmc.org/) for CHD patient recruitment. Whole genome sequencing was performed on Illumina Hi-Seq X Ten machines.
Data analysis	Software used in data analysis included GATK (https://www.broadinstitute.org/gatk/); FreeBayes (https://github.com/ekg/freebayes); DeepSEA (http://deepsea.princeton.edu/); R version 3.4.1; Python versions 2.7 and 3.5. Documentation, links, and availability of source code and select supplementary data is detailed at https://github.com/frichter/wgs_chd_analysis. DNV identification is available at https://github.com/ShenLab/igv-classifier and https://github.com/frichter/dnv_pipeline. The HeartENN algorithmic framework is available at https://github.com/FunctionLab/selene/archive/0.4.8.tar.gz. HeartENN model weights and scripts for burden tests are available at https://github.com/frichter/wgs_chd_analysis. All source code is distributed under the MIT license.

For manuscripts utilizing custom algorithms or software that are central to the research but not yet described in published literature, software must be made available to editors/reviewers. We strongly encourage code deposition in a community repository (e.g. GitHub). See the Nature Research guidelines for submitting code & software for further information.

Data

Policy information about availability of data

All manuscripts must include a data availability statement. This statement should provide the following information, where applicable:

- Accession codes, unique identifiers, or web links for publicly available datasets
- A list of figures that have associated raw data
- A description of any restrictions on data availability

Whole genome sequencing data were deposited in the database of Genotypes and Phenotypes (dbGaP) under accession numbers phs001194.v2.p2 and phs001138.v2.p2.

Field-specific reporting

Please select the one below that is the best fit for your research. If you are not sure, read the appropriate sections before making your selection.

☒ Life sciences ☐ Behavioural & social sciences ☐ Ecological, evolutionary & environmental sciences

For a reference copy of the document with all sections, see nature.com/documents/nr-reporting-summary-flat.pdf

Life sciences study design

All studies must disclose on these points even when the disclosure is negative.

Sample size	No calculation for sample size was performed. Cohort size was determined using samples that had undergone whole genome sequencing. Sample sizes were deemed sufficient based on effect size, statistical significance, and robustness of results across multiple computational and laboratory methods.
Data exclusions	Exclusion criteria were pre-established. Individuals with aneuploidies, structural variants, or likely causal variants in coding regions known to be associated with congenital heart disease were excluded. Controls with possible CHD were also excluded.
Replication	No replication
Randomization	CHD: Presence of structural congenital heart disease Control: Unaffected sibling or parent of proband with autism; ascertained for absence of autism
Blinding	No blinding. Investigators were aware of case-control status, which was required to perform analyses. HeartENN was developed in a blinded fashion (i.e., the investigators did not use patient mutation data for model development).

Reporting for specific materials, systems and methods

We require information from authors about some types of materials, experimental systems and methods used in many studies. Here, indicate whether each material, system or method listed is relevant to your study. If you are not sure if a list item applies to your research, read the appropriate section before selecting a response.

Materials & experimental systems

n/a	Involved in the study
☒	☐ Antibodies
☐	☒ Eukaryotic cell lines
☒	☐ Palaeontology
☒	☐ Animals and other organisms
☐	☒ Human research participants
☒	☐ Clinical data

Methods

n/a	Involved in the study
☒	☐ ChIP-seq
☒	☐ Flow cytometry
☒	☐ MRI-based neuroimaging

Eukaryotic cell lines

Policy information about cell lines

Cell line source(s)	PGP1 cell line was a gift from Church lab. GFP tagged TTN line (doi: 10.1002/cphg.53) was generated from PGP1 in the lab.
Authentication	Pluripotency of the cells were confirmed by their ability to differentiate into beating cardiomyocytes.
Mycoplasma contamination	All cell lines tested negative for mycoplasma contamination.
Commonly misidentified lines (See ICLAC register)	No commonly misidentified cell lines were used.

Human research participants

Policy information about studies involving human research participants

Population characteristics	763 patients and their parents were included in the study. This cohort comprised patients with whole genome sequencing data and congenital heart disease, including atrial septal defects, conotruncal abnormalities, left-sided obstructive lesions, and heterotaxy. There were no exclusion criteria based on age or sex. Phenotypic and genomic data from 1611 unaffected subjects and their parents, not recruited through this study, were obtained through the Simons Foundation.
Recruitment	Patients with structural CHD and their parents were enrolled in the PCGC's Congenital Heart Disease Network Study (CHD

Recruitment	GENES: ClinicalTrials.gov identifier NCT0119618). Selection bias could occur with over-sampling familial CHD, but this risk of bias was minimized through recruitment at >7 institutions in multiple states/countries.
Ethics oversight	The protocols were approved by the Institutional Review Boards of Boston's Children's Hospital, Brigham and Women's Hospital, Children's Hospital of Los Angeles, Children's Hospital of Philadelphia, Columbia University Medical Center, Great Ormond Street Hospital, Icahn School of Medicine at Mount Sinai, Rochester School of Medicine and Dentistry, Steven and Alexandra Cohen Children's Medical Center of New York, and Yale School of Medicine.

Note that full information on the approval of the study protocol must also be provided in the manuscript.